Research paper

Synthesis, characterization and antimicrobial activities of Co(III) and Ni(II) complexes with 5-methyl-3-formylpyrazole-N(4)-dihexylthiosemicarbazone (HMP_zNHex_2): X-ray crystallography and DFT calculations of $[Co(MP_zNHex_2)_2]ClO_4 \cdot 1.5H_2O$ (I) and $[Ni(HMP_zNHex_2)_2]Cl_2 \cdot 2H_2O$ (II)

Manan Saha, Jayanta Kumar Biswas, Monojit Mondal, Debarati Ghosh, Susmita Mandal, David B. Cordes, Alexandra M.Z. Slawin, Tarun Kanti Mandal, Nitis Chandra Saha

PII: S0020-1693(17)31062-9
DOI: https://doi.org/10.1016/j.ica.2018.08.024
Reference: ICA 18424

To appear in: *Inorganica Chimica Acta*

Received Date: 7 July 2017
Revised Date: 19 August 2018
Accepted Date: 19 August 2018

Please cite this article as: M. Saha, J.K. Biswas, M. Mondal, D. Ghosh, S. Mandal, D.B. Cordes, A.M.Z. Slawin, T.K. Mandal, N.C. Saha, Synthesis, characterization and antimicrobial activities of Co(III) and Ni(II) complexes with 5-methyl-3-formylpyrazole-N(4)-dihexylthiosemicarbazone (HMP_zNHex_2): X-ray crystallography and DFT calculations of $[Co(MP_zNHex_2)_2]ClO_4 \cdot 1.5H_2O$ (I) and $[Ni(HMP_zNHex_2)_2]Cl_2 \cdot 2H_2O$ (II), *Inorganica Chimica Acta* (2018), doi: https://doi.org/10.1016/j.ica.2018.08.024

Synthesis, characterization and antimicrobial activities of Co(III) and Ni(II) complexes with 5-methyl-3-formylpyrazole-N(4)-dihexylthiosemicarbazone (HMP_zNHex_2): X-ray crystallography and DFT calculations of $[Co(MP_zNHex_2)_2]ClO_4 \cdot 1.5H_2O$ (**I**) and $[Ni(HMP_zNHex_2)_2]Cl_2 \cdot 2H_2O$ (**II**)

Manan Saha[a], Jayanta Kumar Biswas[b], Monojit Mondal[b], Debarati Ghosh[b], Susmita Mandal[a], David B. Cordes[c], Alexandra M.Z. Slawin[c], Tarun Kanti Mandal[d], Nitis Chandra Saha[a,*]

[a] *Department of Chemistry, University of Kalyani, Kalyani-741 235, India*

[b] *Department of Ecological Studies and International Centre for Ecological Engineering, University of Kalyani, Kalyani-741 235, India*

[c] *School of Chemistry, University of St Andrews, North Haugh, St Andrews, Fife, KY16 9ST U.K.*

[d] *Faculty Councils for Post Graduate Studies, Vidyasagar University, Midnapore-721 102, India*

Abstract

A new pyrazole containing ligand, 5-methyl-3-formylpyrazole-N(4)-dihexylthiosemicarbazone (HMP_zNHex_2), and a host of its cobalt(III) and nickel(II) complexes, $[Co(MP_zNHex_2)_2]X \cdot mH_2O$ and $[Ni(HMP_zNHex_2)_2]X_2 \cdot nH_2O$ (X= Cl, Br, ClO_4, BF_4 and NO_3; m = 0 for Cl, Br, BF_4 & NO_3 and 1.5 for ClO_4; n = 0 for Br, ClO_4, BF_4 & NO_3 and 2 for Cl), respectively, have been synthesized and characterized by elemental analyses, magnetic measurements (polycrystalline state), ^{1}H NMR (for the ligand and its Co(III) complexes), electronic and IR spectral parameters. All the reported Co(III) and Ni(II) complexes are cationic in nature and behaving as 1:1 and 1:2 electrolytes, respectively, in MeOH. Electronic spectral data of the complexes categorize them as having distorted octahedral coordination geometry. IR spectral features (4000-/450 cm^{-1}) specify a monodeprotonated / neutral tridentate (NNS) function of the ligand, HMP_zNHex_2 coordinating to the Co(III) / Ni(II) via the pyrazolyl (tertiary) ring nitrogen, azomethine nitrogen and thiolato / thioketo sulfur atom. ^{1}H NMR spectral data (in $CDCl_3$ at 400 MHz) for the primary ligand and those of its Co(III) complexes are in agreement with the proposition of bonding sites evidenced from IR data. The single crystal x-ray data of **I** (C2/c (#15); monoclinic) and **II** (P-1 (#2); triclinic) have confirmed a CoN_4S_2 and a NiN_4S_2 octahedral coordination, respectively. The pair of monoprotic / neutral coordinating ligands

is more or less orthogonal to each other in the complex species. The data obtained from DFT calculations are reasonably in agreement with the UV-Vis spectral assignment and the structures of the complex species. Although the ligand and the tested metal ion complexes are capable of inhibiting microbial growth, the cobalt complexes can be promoted as better antimicrobial agents.

Keywords: Cobalt(III) complexes; Nickel(II) complexes; Thiosemicarbazone; X-ray crystallography; Antimicrobial activities.

---

*Corresponding author. Fax: +91-33-25828282; e-mail: nitis.saha@gmail.com

1. Introduction:

A plethora of literature on thiosemicarbazones has been published wherein different aspects of their coordination behavior leading to excellent biological activities viz., antitumor, antibacterial, fungicidal, anti-inflammatory, antiviral, anticancer, antifungal and anti-HIV activity etc. are discussed [1-16]. Thiosemicarbazones are an outstanding class of multidentate ligands, comprising of potential binding sites accessible to different types of metal ions and with a wide range of analytical applications [17]. The well established biological activities of thiosemicarbazone class of compounds are often related to their chelating ability with transition metal ions, bonding through N, N, and S atoms [18] or O, N and S atoms [3,19,20]. It has been observed that the substituent(s) present at the N(4)-position affect the activity of the thiosemicarbazones and their metal ion complexes [21]. A bulky substituent present at the N(4) position of the thiosemicarbazone chain might bring about an enhancement of antimicrobial activity compared to an un-substituted one, possibly due to an increase in lipophilicity, which influences the tendency of a molecule to be transported through biological membranes [22a]. On the other hand, different counter anions present in the complexes of a particular metal ion play definitive roles in enhancement of biological activities [22b,c]. In recent years, Co(III) thiosemicarbazone complexes have drawn much attention as anticancer drugs and potential hypoxia-activated pro-drugs [23-31]. Ni(II) thiosemicarbazone complexes containing multiple donor sites have now been more comprehensively studied for their fascinating structural diversities and wide applications as antibacterial, antifungal and anticancer agents [32-43]. A variety of factors can be cited to be accountable for their flexibility in coordination, such as intramolecular hydrogen bonding, bulkier coligand, steric crowding on the azomethine carbon atom and π–π stacking interactions [44-49]. A potential donor atom or a functional group which is capable of furnishing a variety of coordination modes, present in the primary ligand systems, plays crucial role in providing flexibility to the ligands which can coordinate to the transition

metal ion in a neutral or deprotonated form, producing mono or poly nuclear complexes with novel topologies and particular properties [50–58]. As a part of syntheses and characterizations of new thiosemicarbazones and their complexes and in continuation of our earlier publications [55, 56], this communication is intended to report the synthesis, physico-chemical & spectroscopic characterization and antimicrobial studies of a series of Co(III) and Ni(II) complexes having different counter ions with the title ligand, HMP_zNHex_2, along with the X-ray crystallography and DFT study of $[Co(MP_zNHex_2)_2]ClO_4 \cdot 1.5H_2O$ (**I**) and $[Ni(HMP_zNHex_2)_2]Cl_2 \cdot 2H_2O$ (**II**).

2. Experimental

All the solvents and reagents used were of reagent grade / molecular biology grade, and used as commercially purchased without further purification. Spectroscopy grade solvents were used for spectral and conductance measurements.

2.1. Physical measurements

Elemental analyses (C, H and N) were done with a Perkin–Elmer 2400 CHNS/O analyzer. The cobalt contents of the complexes were determined by complexometric titration using EDTA, while the nickel contents of the complexes were determined gravimetrically as anhydrous dimethylglyoximatonickel(II). The molar conductance of the complexes in methanol solutions was measured with a Systronics 306 digital conductivity meter. Magnetic susceptibilities of the complexes in polycrystalline state were measured on a PAR 155 sample vibrating magnetometer. ^{1}H NMR spectra for the ligand and cobalt(III) complexes were recorded with a Bruker AC 400 superconducting FT NMR spectrometer. High resolution mass spectroscopy (HRMS) was performed with a Waters XEVO G2-S QTof mass spectrometer. The electronic spectra (in MeOH) were recorded on a Shimadzu UV-2401PC spectrophotometer. IR spectra

(4000–400 cm^{-1}) were recorded on a Perkin Elmer L120-000A FT-IR spectrophotometer with KBr pellets.

2.2. Synthesis of 5-methyl-3-formylpyrazole-N(4)-dihexylthiosemicarbazone (HMP_zNHex_2):

The title ligand, 5-methyl-3-formylpyrazole-N(4)-dihexylthiosemicarbazone (HMP_zNHex_2) (Fig.1a), was synthesized following a similar but suitably modified method [59a]. Which involved conversion of 5-methylpyrazole-3-carbohydrazide [59b] into its benzene sulphonyl derivative, followed by treatment with the S-methyldithiocarbazate [59c] in alkaline ethylene glycol medium (160°C) leading to the pale yellow solid S-methyldithiocarbazate of 5-methyl-3-formylpyrazole (HMP_zSMe). Finally the transamination [60] of resulting HMP_zSMe with dihexylamine, gave the desired product. White crystallised product (from ethanol) obtained with a yield of ~75%, melted at 159-160^{0}C. Anal. Found: C, 61.6; H, 9.4; N, 19.8; Calc. for $C_{18}H_{33}N_5S$: C, 61.5; H, 9.5; N, 19.9%. HRMS m/z: Calc. for $C_{18}H_{33}N_5S$ $[M+H]^+$ 352.5611, found 352.2650. IR (KBr): ν (cm^{-1}) = 3165(ν_{NH}), 1604 ($\nu_{CH=N,}$ azomethine), 1499 ($\nu_{C=N,}$ pyrazole), 1087 (ν_{N-NPZ}) and 869 ($\nu_{(C=S)}$). ^{1}H NMR ($CDCl_3$) δ(ppm): 12.83 (s, 1H, NH pyrazole); 11.51 (s, 1H, NH imino), 7.27 (s, 1H, CH=N), 2.34 (s, 3H, C_5-CH_3), 6.12 (s, 1H, C_4-H), 3.64 (t, 4H), 1.65 (m, 4H), 1.23 (m, 12H), 0.79 (t, 6H).

2.2.1. Preparation of the Co(III) and Ni(II) complexes

The reported Co(III) and Ni(II) complexes (Figs. 1b and 1c) of the title ligand, HMP_zNHex_2 were prepared by refluxing ethanol solutions of the ligand, (1.05 mmol) and the corresponding hydrated Co(II) or Ni(II) salts (0.525 mmol) in water bath for ~1 h. The desired Co(III) or Ni(II) complexes, in each case, crystallized out on slow evaporation of the dark brown or green solutions, respectively. The solids obtained were filtered off, washed with cold ethanol and were dried over anhydrous $CaCl_2$. The yields of the products were found to be ~75-80%. Orange crystals of $[Co(MP_zNHex_2)_2]ClO_4 \cdot 1.5H_2O$ (**I**) and green crystals of

$[Ni(HMP_zNHex_2)_2]Cl_2 \cdot 2H_2O$ (**II**) were found suitable for X-ray diffraction study. Anal. Calc. (%) for $C_{36}H_{67}ClCoN_{10}O_{5.5}S_2$ (**I**): C, 48.8; H, 7.3; N, 15.8; Co, 6.6. Found (%): C, 48.7; H, 7.2; N, 15.7; Co, 6.7. HRMS m/z: Calc. for $C_{36}H_{64}N_{10}S_2Co$ $[M-(ClO_4+1.5H_2O)]^+$ 759.4088, found 759.3989. IR (KBr): ν (cm^{-1}) =1575 ($\nu_{CH=N}$, azomethine), 1505 ($\nu_{C=N}$, pyrazole), 1146 (ν_{N-NPZ}) and 809 ($\nu_{(C=S)}$). UV-Vis (MeOH, λ_{max}, nm): 227 ($\pi \rightarrow \pi^*$), 325 ($n \rightarrow \pi^*$), 391 (LMCT). ^1H NMR ($CDCl_3$) δ(ppm): 12.99 (s, 1H, NH pyrazole), 8.39 (s, 1H, CH=N), 2.59 (s, 3H, C_5-CH_3), 6.17 (s, 1H, C_4-H), 3.74 (t, 4H), 1.67 (m, 4H), 1.27 (m, 12H), 0.89 (t, 6H).

Anal. Calc. (%) for $C_{36}H_{70}Cl_2N_{10}NiO_2S_2$ (**II**): C, 49.8; H, 7.6; N, 16.1; Ni, 6.8. Found (%): C, 49.3; H, 7.4; N, 16.4; Ni, 6.9. HRMS m/z: Calc. for $C_{36}H_{66}N_{10}S_2Ni$ $[M-(2Cl+2H_2O)]^+$ 761.7996, found 761.4103. IR (KBr): ν (cm^{-1}) = 1562 ($\nu_{CH=N}$, azomethine), 1514 ($\nu_{C=N}$, pyrazole), 1129 (ν_{N-NPZ}) and 846 $\nu_{(C=S)}$. UV-Vis (MeOH, λ_{max}, nm): 223 ($\pi \rightarrow \pi^*$), 307 ($n \rightarrow \pi^*$), 359 (LMCT).

Caution! Metal ion complexes with organic ligands containing perchlorate as anion are potentially explosive and should be handled with care.

2.3. Structure determination

X-ray diffraction data for compounds **I** and **II** were collected at 125 K using the St Andrews Automated Robotic Diffractometer (STANDARD) [61], consisting of a Rigaku sealed-tube generator, equipped with a SHINE monochromator [MoKα radiation (λ = 0.71075Å)] and a Saturn 724 CCD area detector, coupled with a Microglide goniometer head and an ACTOR SM robotic sample changer. Intensity data were collected using ω steps accumulating area detector images spanning at least a hemisphere of reciprocal space. All the data were corrected for Lorentz polarization effects. A multiscan absorption correction was applied by using CrystalClear [62]. Structures were solved by direct (SIR2004 [63]) or charge-flipping (Superflip [64]) methods and refined by full-matrix least-squares against F^2 (SHELXL-2013 [65]). Non-

hydrogen atoms were refined anisotropically, and hydrogen atoms were refined using a riding model, except for N-H hydrogens in **I** which were located from the difference Fourier map and refined isotropically subject to a distance restraint. Due to the data-quality in **II** the equivalent hydrogens could not be located. Disorder was found in the orientation of the ClO_4^- anion in **I**, in one C_6 chain in **I**, and in parts of two of the C_6 chains in **II**. All cases of disorder were modelled with split atom positions, and the minor components of the disorder, except the disordered Cl in **I**, were refined isotropically. Both cases of disorder in **I** were modelled with distance and angle restraints as well as similarity restraints to thermal motion parameters, while the disorder in **II** required with similarity restraints on thermal motion only. Despite modelling disorder with split atom positions in **I**, thermal ellipsoids for the major components of the disordered atoms remained large, suggesting that further disorder was present; however this could not be successfully refined. Compound **II** was affected by non-merohedral twinning, with a twin law of [-1 0 0 0.01 1 -0.352 0 0 -1] and a refined twin fraction of 0.41. There were suggestions that further twinning might also be occurring, but this could not be successfully incorporated into the model. All calculations were performed using the CrystalStructure [66] interface.

2.4. Computational details

All the quantum chemical calculations were performed using density functional theory (DFT) implemented in GAUSSIAN 09 [67]. The geometry of the complex-**I** and complex-**II** were fully optimized using M062X hybrid functional and 6-31g (d, p) basis set. The absorption spectra were simulated using Time Dependent Density Functional Theory (TD-DFT). All the computational study was carried out in Methanol solvent using Polarizable Continuum Model (PCM) implemented in Gaussian 09. The orbital contribution was calculated by GaussSum [68].

2.5. Antimicrobial activity

All the 11 synthetic compounds were dissolved in dimethyl sulfoxide, (DMSO), while maintaining final solvent concentration up to 1%. Amoxicillin, a clinically recommended antibacterial agent was employed as the reference material [56]. *In vitro* antimicrobial potential of all the synthetic compounds under investigation were evaluated against three Gram negative bacterial strains, namely *Salmonella enterica ser. typhi* SRC, *Proteus vulgaris* OX19, *Enterobacter aerogenes* 10102 and one Gram positive bacterial strain (*Bacillus subtilis* 6633), which were obtained from Microbial Type Culture Collection and Gene Bank (MTCC), Institute of Microbial Technology, Chandigarh, India. Minimum inhibitory concentrations (MIC) of the compounds were determined by tube dilution method with different concentrations of them as per standard protocol [69]. Different concentrations of all the compounds were made in sterilized LB broth and then overnight culture of individual bacterial strain was inoculated into respective tubes and incubated at 37°C for 24 hours. The activity was measured by turbidity in the broth with UV-Vis spectrophotometer at 600nm. Bacterial susceptibility of the compounds was assessed following agar well diffusion method and the degree of inhibition was determined by measuring the diameter of inhibition zones (mm) [70]. Two strains, one Gram positive and one Gram negative (*Bacillus subtilis* 6633 and *Enterobacter aerogenes* 10102) were monitored for the study of growth kinetics in presence of the compounds.

3. Results and discussion:

3.1. Spectroscopic characterization of the ligand, HMP_zNHex_2

The title ligand, HMP_zNHex_2 was characterized by elemental analyses (C, H and N), IR, ^1H NMR and high resolution mass spectral (HRMS) studies. The characteristic IR bands (cm^{-1}) at 3165 (ν_{NH}), 1604 ($\nu_{(CH=N)}$), 1499 ($\nu_{(C=N)}$), 1087 ($\nu_{N\text{-}NPZ}$) and 869 ($\nu_{(C=S)}$) were in good agreement with the structure in Fig.1. The ^1H NMR spectrum of the free ligand in $CDCl_3$ furnished singlets

at δ = 2.34 (3H), 6.12 (1H), 12.83 (1H), 7.27 (1H) and 11.51(1H) assigned to C_5-CH_3, C_4-H, N^1-H of the pyrazole ring, -CH=N and NH imino, respectively. The spectrum also showed triplets at δ = 3.64 (4H) and 0.79 (6H); multiplets at δ = 1.65 (4H) and 1.23 (12H) ascribed for the dihexyl side chain.

3.2. Characterization of the Co(III) and Ni(II) complexes

All the metal ion complexes, reported here, gave satisfactory C, H, N and metal analyses, and corroborated to the general composition: $[Co(MP_zNHex_2)_2]X\cdot mH_2O$ and $[Ni(HMP_zNHex_2)_2]X_2\cdot nH_2O$ *(X= Cl, Br, ClO_4, BF_4 and NO_3; m =1.5 for ClO_4 and n = 2 for Cl)*. The Co(III) and Ni(II) complexes behaved as 1:1 and 1:2 electrolytes, respectively, in methanol (30^0C) [71]. As expected, all the spin-paired Co(III) complexes reported here are diamagnetic (at ~/300 K) in nature, while the normal spin free Ni(II) complexes are paramagnetic with magnetic moments μ_{eff} =/2.89-3.20 BM (Table 1).

3.2.1 Spectral studies

3.2.1.1 IR spectroscopy

A comparison of the characteristic IR bands of the free ligand with those of its metal ion complexes, reported here, offered positive indications regarding the bonding sites of the primary ligand. A negative shift was found to occur in ($\upsilon_{CH=N}$) band (1604 cm^{-1}) in the free ligand spectrum to the lower value (1557-1575 cm^{-1}) (Table S1) in its complexes, pointed out coordination of the azomethine nitrogen to the central metal ion; the appearance of IR bands at 469-/497 cm^{-1} in the spectra of the complexes can then be assigned to υ(M-N) [54a]. The IR band obtained at 1499 cm^{-1} in the free ligand spectrum, assignable to $\upsilon_{(C=N)}$ (pyrazole ring), has been found to suffer positive shift to higher frequency region 1504 – 1516 cm^{-1} in complex species, indicating the participation of the tertiary ring nitrogen atom (^{2}N) as a possible bonding site. IR

band observed at 1087 cm^{-1} ($\nu_{N\text{-}NPZ}$) in the primary ligand, was also found to shift to a higher frequency region 1129 – 1146 cm^{-1} in complexes, which provided further information of the participation of the tertiary ring nitrogen atom (^{2}N) in bonding [55,56,72,73]. A strong band appeared at 869 cm^{-1} in the free ligand spectrum, assigned to $\upsilon_{(C=S),}$ had been found to shift to lower frequency region (797-847 cm^{-1}) in the complexes, pointing towards coordination of the sulfur in its thioenol or thioketo form to metal ion [54].

3.2.1.2 Electronic spectroscopy and TD-DFT study

The electronic spectra of the Co(III) complexes in MeOH solution exhibited two bands in the regions 225-229 and 324-325 nm, which might be ascribed to intraligand π→π* and n→π*, transitions, respectively [74a, 75-76]. The spectra also displayed a shoulder at 389-393 nm, possibly due to S→Co(III) charge transfer bands (LMCT) [54a]. The UV–Vis absorption spectra of Ni(II) complexes in methanol displayed two bands in the region 203-223 and 297-307 nm, might be assigned for intraligand π→π* and n→π* transitions, respectively [74b, 76]. The shoulder found at 359-360 nm might be due to S→Ni(II) charge transfer bands (LMCT) [54a] .

TD-DFT calculation was performed on complexes **I** and **II** (as reference) to explain the experimental absorption spectra. The experimental UV–Vis data are reasonably in agreement with the quantum chemical calculations from the TD-DFT study. The vertical excitations with their band position, oscillator strength and character assignment of the transition from TDFT are given in (Table 2). In complex **I**, the simulated transitions at 234.97 nm (λ_{exp} = 227.82 nm) and 292.93 nm (λ_{exp} = 325.51 nm) are correspond to intraligand transition bands (π→π* and n→π* respectively). The peak resolved theoretically at 359.67 nm resembles the shoulder obtained experimentally (λ_{exp} = 391.49 nm) and can be assigned a S→Co(III) charge transfer bands (LMCT) (Fig. 2). Similarly, for complex **II**, all the experimentally resolved peaks are reasonably

in agreement with the simulated peaks (Fig. 3). The compositions and energies of the frontier molecular orbitals of the complex are given in Tables S2 & S3.

3.2.1.3 ^{1}H NMR spectral study

^{1}H NMR spectral data of the free ligand and those of its Co(III) complexes are summarized in Table 3. A close scrutiny of the data revealed that: (i) After complexation, the disappearance of the imino ^{2}NH (at the thiosemicarbazone part in the free ligand molecule) peak at δ =/11.51, signifying that the ligand experienced deprotonation and coordinated to the Co(III) ion through the thiol sulfur. (ii) The peaks for terminal -N(n-Hex_2)$_2$ groups in the uncomplexed ligand suffered little down-field shifts in the complex species, which is indicative of coordination of the thiol sulfur to Co(III) ion, due to which reduction of electron density at the terminal N-atom of N(n-Hex_2)$_2$ occurred. (iii) Peak at δ = 7.27 due to azomethine CH proton in the free ligand, experienced maximum downfield shift in the complex species (δ = 8.39-8.44), pointing to the coordination of the azomethine nitrogen to the Co(III) ion. (iv) ^{4}CH (pyrazole ring) suffered down field shift from δ = 6.12 (free ligand) to δ = 6.15-6.19 in the complexes justified the coordination of the pyrazole ring ^{2}N (tertiary) to the Co(III) ion. ^{1}H NMR spectral studies, thus, authenticated the binding modes of the primary ligand, HMP_zNHex_2 in forming complexes with Co(III), through the pyrazolyl ring nitrogen ^{2}N (tertiary), azomethine nitrogen and thiolato sulfur atom [55,56], as ascertained from the IR spectroscopic data.

*3.3. Crystal structures of $[Co(MP_zNHex_2)_2]ClO_4{\cdot}1.5H_2O$ (**I**) and $[Ni(HMP_zNHex_2)_2]Cl_2{\cdot}2H_2O$ (**II**)*

Views of the X-ray structures of the complexes (**I** and **II**) together with the atom numbering schemes were shown in Figs. 4 and 5. The crystallographic data and refinement parameters were summarized in Table 4. A $[Co(MP_zNHex_2)_2]^{+}$ cation, a ClO_4^{-} anion and 1.5 molecules of water

of crystallization formed the crystallographic asymmetric unit in **I**; whereas the same in **II** had been constituted by a $[Ni(MP_zNHex_2)_2]^{++}$ cation, two Cl^- anions and two molecules of water of crystallization. In both **I** and **II** the central metal ions had distorted octahedral coordination, the distortion being more prominent in the Ni(II) complex (Table 5). A pair of mono-deprotonated ligands, ($MP_zNHex_2^-$), was found to coordinate to the Co(III) ion through the pyrazolyl (tertiary) ring nitrogen atoms [N1, N31], the hydrazinic chain nitrogen atoms [N8, N38], and the thiolato sulfur atoms [S10, S40] in complex **I**. On the other hand, the mode of coordination in complex **II** remained the same; with the exception that the pair of coordinating ligands did not undergo deprotonation and behaved as neutral species. In both complexes **I** and **II**, two molecules of the NNS tridentate ligand, in either mononegative or neutral forms, respectively, coordinated to the metal ion to form four five-membered chelate rings (M-S10-C10-N9-N8, M-S40-C40-N39-N38, M-/N1-C5-C7-N8 and M-N31-C35-C37-N38; M = Co, Ni). The two azomethine nitrogen atoms, N8 & N38, were oriented *trans* to each other, while both the pyrazolyl ring nitrogen atoms, N1 & N31, and the sulfur atoms, S10 & S40, were in a *cis* orientation.

The lessening of the endocyclic angles at the hydrazinic nitrogens, N9 and N39, in complex **I**, might be due to deprotonation, occurred at these points; no such reduction was found to happen with the corresponding angles in complex **II**, where no deprotonation occurred at the hydrazinic nitrogen atoms (Table 5). As a result of which, the double bond character of the N9-C10 & N39-C40 bonds in complex **I** was enhanced with subsequent decrease in the double bond character of the C10-S10 & C40-S40 bonds; this had not been observed in complex **II,** where deprotonation did not occur. In both **I** and **II**, the reduction in the bond distances formed between the metal ions and the azomethine nitrogen atoms, N8 & N38, in comparison to the bond distances with the pyrazolyl (tertiary) ring nitrogen atoms, N1 & N31 (Table 5), might be ascribed by the fact that among the azomethine nitrogen and the pyrazolyl nitrogen, the former was as a stronger base.

Table 6 provided the details of the hydrogen bonding interactions prevailed in the structures. All the potential hydrogen donors, namely, the pyrazolyl secondary nitrogen atoms (N2 and N32) in both complex **I** & **II**, and the hydrazinic nitrogen atoms (N9 and N39) in complex **II**, were engaged in classical hydrogen bond formation with the water, perchlorate oxygen and chlorine atoms. While the hydrogen atoms on water molecules could not be located, details of hydrogen bonding can be deduced from the positioning of the waters in the cases in **I** and **II**, and the nature of the resulting hydrogen-bonded supramolecules determined. In **I**, a two dimensional hydrogen-bonded network was formed in the (1 0 0) plane, comprising one dimension chains of hydrogen-bonded water molecules and perchlorate anions, linked together by complex cations. In **II** a simple one-dimensional hydrogen-bonded chain had been formed, running along the crystallographic *ac* diagonal axis. The hydrogen bonding and crystallographic packing of the complexes was shown in Figs. 6 and 7.

Computational study was performed using density functional theory (DFT) with M062X hybrid functional and 6-31g (d, p) basis set to optimize the geometry of complexes **I** and **II**. Both the octahedral complexes were fully optimized (Fig. 8). A comparison of the bond length and bond angles between the experimental and the optimized structures of both the complexes is given in Table 5. The harmony between the crystal structures and the optimized structures indicates that the level of calculation is fairly good for this type of molecules.

3.4. Antimicrobial activity

The study revealed that all the synthesized compounds and the ligand inhibited microbial growth. The respective MIC values and growth inhibition zone diameters for these compounds were presented in Tables 7 and 8. Although the ligand (MS1) exhibited potential antibacterial activity against all four bacterial strains with MIC values within the range of 200 to 500 μg mL^{-1}, it was found most effective against *B. subtilis* 6633 and *P. vulgaris* OX19, with the MIC values of 200

and 300 μg mL^{-1}, respectively. The reported cobalt compounds (MS2, MS3, MS4, MS5 and MS6) showed antibacterial activities against all Gram-positive and Gram-negative bacteria, with MIC range of 225 to 1675 μg mL^{-1}. On the other hand five nickel compounds (MS7, MS8, MS9, MS10 and MS11) also exhibited a wide range of antibacterial activity with comparatively higher MIC values (775 - 1650 μg mL^{-1}). It suggests that the cobalt complexes possess greater antimicrobial potential compared to the nickel complexes. Further the anionic groups contributed to the antimicrobial potential of the complexes more evident in case of the Co(III) complexes in the following order of variation: fluoroborate > perchlorate > nitrate > bromide > chloride. In case of Ni(II) complexes, the maximum antibacterial activity was conferred by fluoroborate followed by perchlorate. In contrast the minimum antibacterial activity was observed in case of chloride, bromide or nitrate against different bacteria. So, it can be concluded that all the synthesized compounds and the ligand tested have varied antibacterial potential against selected representatives from both Gram positive and Gram negative categories. It might have some connotations for their wide window of antibacterial activities.

Agar well diffusion study showed that MS3, 4, 7, 8, 10, 11 showed higher antimicrobial efficiency against *S. typhi*, MS1, 2, 5, 9 against *E. aerogenes* and MS2, 6 against *B. subtilis* as evident from the respective inhibition zone diameters. This also finds support from degree of growth restriction evident in the bacterial growth kinetics. The cobalt compound MS2 was found effective against both Gram positive (*B. subtilis*) and Gram negative (*E. aerogenes*). *P. vulgaris* showed the least vulnerability to majority of the complexes (MS1, 2, 3, 4, 10, 11). *S. typhi* offered higher tolerance against two cobalt compounds (MS5 and 6) while *B. subtilis* against two nickel compounds (MS7, 8). It is noteworthy that one nickel compound (MS 11) offered the highest growth inhibition zone against *S. typhi*. No concrete inference on the comparative efficiencies of tested complexes can be drawn based on the growth inhibition zone diameters

derived from the agar well diffusion study because of the fact that the concentrations of the selected Co- and Ni- complexes were different and set at respective MICs.

Growth kinetics study performed with two different bacterial species (*Enterobacter aerogenes* 10102 and *Bacillus subtilis* 6633) subjected to the synthetic compounds presented significant growth inhibition induced by these chemical candidates as illustrated by the *in vitro* growth curves (Figs. 9 and 10). In the control set in absence of any complex or standard antibiotic *Bacillus subtilis* 6633 (a Gram positive bacterial strain) showed an exponential growth pattern up to 12 hour followed by a stationary phase. When subjected to cobalt and nickel compounds growth was dampened immediately under exposure to MS 4, 6, 8 that continued up to 2nd hour. In case of MS1, 2, 3, 9, 10 marked decline in growth rate was observed between 2nd and 4th hour of incubation. Against MS 11 the bacteria showed dampened growth all through after 6th hour onwards. High recovery in growth of the bacteria was witnessed in presence of all cobalt compounds (MS2, 3, 4, 5, 6) and one nickel compound (MS7). In contrast low rates of growth recovery were observed for the bacteria in presence of all the nickel compounds (MS8, 9, 10 and 11, except MS7) and MS1. There observed significant variations (P<0.05) among the nickel compounds in restricting growth in the following order: MS11 > MS10 > MS9 > MS8 showing their relative bacteriostatic efficiency. For *Enterobacter aerogenes* 10102 (a Gram negative bacterial strain) in the control set in absence of any complex or standard antibiotic showed an exponential increase in growth up to 18 hour without any stationary phase during the course of incubation. Immediate bacteriostatic effect was reflected for majority of compounds (MS1, 4-11) that persisted for 2-4 hours but bacterial growth rate was declined between 2nd to 4th hours against MS2, 3. The highest degrees of dampened growth were observed against certain nickel compounds (MS7, 8, 9) showing relative bacteriostatic efficiency of those compounds. The bacterial strain recovered the growth potential against all compounds except the one nickel

compound (MS9) and the ligand (MS1) implying the highest antibacterial efficiency of MS9 against *E. aerogenes*. From the study on bacterial growth kinetics in presence of the tested compounds as well as the ligand it was evident that the compounds offered varied potential for inhibiting bacterial growth and therefore they may be promoted as bacteriostatic agents depending on the class and species of the pathogenic bacteria.

The compounds tested in the present study might have increased the permeability of the cell membranes which has led the compounds to penetrate the cell and cause bacterial growth inhibition or death. It has been found that enhancement of antimicrobial activity occurred for a thiosemicarbazone complex containing a bulkier substituent present at the N(4) position compared to an un-substituted one or one containing less bulkier substituent. The presence of the bulkier substituent is possibly responsible for an increase in lipophilicity of the complex, which influences the tendency of a molecule to be transported through biological membranes [22].

Although the present study does not show any direct experimental evidence about the mechanism of antibacterial activity of the Co and Ni complexes, it can be corroborated with our previous observation of membrane damage as inflicted by some Ni, Cd and Hg complexes against Gram positive (*Bacillus subtilis* 6633) and Gram negative (*Proteus vulgaris* OX19) bacterial strain [77]. In such cases the complexes might have caused membrane damage and consequent physiological disruption and bacteriostatic/bactericidal action. Such antimicrobial activity may arise on coordination to the metal ion and can be explained in terms of Overtone's concept of cell permeability [78] and Tweedy's chelation therapy [79]. According to the former concept, the lipid membrane surrounding the cell favors the passage of only lipid-soluble materials which thereby enhance the lipophilic character and thereby the complexes enable interaction with the cell constituents. On the other hand, chelate formation reduces the polarity of the metal centre to a considerable extent due to overlapping of the ligand orbital and partial sharing of the positive charge of the metal ion with the donor atoms. Also the rigidity of the primary ligand molecule in

the complexes may facilitate the interaction [80, 81]. Nonetheless, soft and borderline metal atoms as well as metal oxy-anions show electron-sharing affinities to facilitate formation of covalent bonds with S and consequent generation of protein disulphides and depletion of antioxidant reserves, particularly glutathione, within the microbial cells [82]. Depletion of total thiols in the cellular environment has been observed under the metal stress condition developed due to some metals like Co(II) following the bacterial exposure to such toxic assault. The enzymes involved in thiol–disulphide homeostasis mediated by glutathione, glutaredoxin and thioredoxin systems are important determinants of bacterial tolerance to all those metals [82, 83]. In other words, synthetic compounds with metal salt anions could deplete the protective antioxidant system of the bacteria and can serve the role of antimicrobial agents.

4. Conclusion:

The present communication deals with the syntheses, spectral characterizations and antibacterial activities of a host of Co(III) and Ni(II) complexes of the ligand, 5-methyl-3-formylpyrazole-N(4)-dihexylthiosemicarbazone, (HMP_zNHex_2), along with the crystal structures and DFT calculations of $[Co(MP_zNHex_2)_2]ClO_4 \cdot 1.5H_2O$ and $[Ni(HMP_zNHex_2)_2]Cl_2 \cdot 2H_2O$. All the reported metal ion complexes are octahedral in nature and the bonding of the primary ligand with Co(III) / Ni(II) centre, in each case, takes place through the pyrazolyl tertiary ring nitrogen atom, azomethine nitrogen atoms and the thiolato/ thione sulphur atoms. It has been found that although the ligand and all the synthesized metal complexes are capable of inhibiting microbial growth as bacteriostatic candidates, the cobalt complexes can be promoted as better antimicrobial agents.

Acknowledgements:

One of us (Manan Saha) is thankful to the U.G.C., Govt. of India for providing financial support in the form of Rajiv Gandhi National Fellowship (Number and date of award letter: F1-17.1/2013-14/RGNF-2013-14-SC-WES- 51398/(SA-III/Website); 06/02/2014). N.C. Saha is thankful to the University of Kalyani for financial assistance received in the form of Personal Research Grant.

Appendix A. Supplementary data

CCDC Nos 1442106 and 1442107 contain the supplementary crystallographic data for **I** and **II**, respectively. These data can be obtained free of charge via http://www.ccdc.cam.ac.uk/conts/retrieving.html, or from the Cambridge Crystallographic Data Centre, 12 Union Road, Cambridge CB2 1EZ, UK; fax: (+44) 1223-336-033; or e-mail: deposit@ccdc.cam.ac.uk. Tables S1-S4 are available as supplementary material.

References:

[1] J.P. Scovill, D.L. Klayman, C.F. Franchino, J. Med. Chem. 25 (1982) 1261.

[2] M.E. Hossain, M.N. Alam, J. Begum, M.A. Ali, M. Nazimuddin, F.E. Smith, R.C. Hynes, Inorg. Chim. Acta 249 (1996) 207.

[3] P. Bindu, M.R.P. Kurup, T.R. Satyakeerthy, Polyhedron 18 (1999) 321.

[4] J. Haribabu, G.R. Subhashree, S. Saranya, K. Gomathi, R. Karvembu, D. Gayathri, J. Mol. Struct. 1110 (2016) 185.

[5] J. Straiat, P. Kovarikova, J. Klimes, D.S. Kalinowski, D.R. Richardson, Anal. Bioanal. Chem. 397 (2010) 161.

[6] Y. Kang, N. Yang, S.O. Kang, J. Ko, Organometallics 16 (1997) 5522.

[7] D. X. West, J. K. Swearingen, J. Valdés-Martínez, S. Hernández-Ortega, A. K. El-Sawaf, F. van Meurs, A. Castiñeiras, I. Garcia, E. Bermejo, Polyhedron 18 (1999) 2919.

[8] P. Tarasconi, S. Capacchi, G. Pelosi, M. Cornia, R. Albertini, A. Bonati, P. P. Dall'Aglio, P. Lunghi, S. Pinelli, Bioorg. Med. Chem. 8 (2000) 157.

[9] A. Kumar, Usha, S. Chandra, Synth. React. Inorg. Met. Org. Chem. 23 (1993) 671.

[10] L.J. Ackerman, P.E. Fanwick, M.A. Green, E. John, W.E. Running, J.K. Swearingen, J.W. Webb, D.X. West, Polyhedron 18 (1999) 2759.

[11] U.P. Singh, R.K. Singh, H.R. Bhat, Y.P. Subhashchandra, V. Kumar, M.K. Kumawat, P. Gahtori, Med. Chem. Res. 20 (2011) 1603.

[12] M.C. Rodríguez-Argüelles, P. Tourón-Touceda, R. Cao, A.M. García-Deibe, P. Pelagatti, C. Pelizzi, F. Zani, J. Inorg. Biochem. 103 (2009) 35.

[13] M. Devereux, D.O. Shea, A. Kellett, M. McCann, M. Walsh, D. Egan, C. Deegan, K. Kędziora, G. Rosair, H. Müller-Bunz, J. Inorg. Biochem. 101 (2007) 881.

[14] E. Türkkan, U. Sayin, N. Erbilen, S. Pehlivanoglu, G. Erdogan, H. U. Tasdemir, A. O. Saf, L. Guler, E. G. Akgemci, Journal of Organometallic Chemistry 831 (2017) 23

[15] T.S. Lobana, S. Indoria, H. Sood, D.S. Arora, B.S. Randhawa, I. Garcia-Santos, V. A. Smolinski, J.P. Jasinski, Inorg. Chim. Acta 461 (2017) 248

[16] F.A. Beckford, K.R..Webb, Spectrochimica Acta Part A: Molecular and Biomolecular Spectroscopy 183 (2017) 158

[17] Diana-Carolina Ilies, S. Shova, V. Radulescu, E. Pahontu, T. Rosu, Polyhedron 97 (2015) 157 and references therein.

[18] A.C. Sartorelli, K.C. Agrawal, A.S. Tisftsoglou, E.C. Moore, Adv. Enzyme Reg. 15 (1977) 117.

[19] Z. Lu, C. White, A.L. Rheingold, R.H. Crabtree, Inorg. Chem. 32 (1993) 3991.

[20] S.K. Dutta, D.B. McConville, W.J. Youngs, M. Chaudhuri, Inorg. Chem. 36 (1997) 2517.

[21] A.E. Liberta, D.X. West, Biometals 5 (1992) 121.

[22](a) E. Keskioglu, A.B. Gunduzalp, S. Cete, F. Hamurcu, B. Erk, Spectrochim. Acta A 70 (2008) 634; (b) Z.H. Chohan, A. Rauf, Metal-Based Drugs, 3 (1996) 211; (c) Z.H. Chohan, A. Rauf, C.T. Supuran, Metal-Based Drugs, 8 (2002) 287.

[23] C.V. Garcia, G.L. Parrilha, B.L. Rodrigues, P.J.S. Barbeira, R.M. Clarke,T. Storr, H. Beraldo, Polyhedron 124 (2017) 86.

[24] I.H. Hall, C.B. Lackey, T.D. Kistler, R.W. Durham, E.M. Jouad, M. Khan, X.D. Thanh, S. Djebbar-Sid, O. Benali-Baitich, G.M. Bouet, Pharmazie 55 (2000) 937.

[25] R. Manikandan, P. Vijayan, P. Anitha, G. Prakash, P. Viswanathamurthi, R.J. Butcher, K. Velmurugan, R. Nandhakumar, Inorg. Chim. Acta 421 (2014) 80.

[26] M.D. Hall, T.W. Failes, N. Yamamoto, T.W. Hambley, Dalton Trans. (2007) 3983.

[27] T.W. Failes, C. Cullinane, C.I. Diakos, N. Yamamoto, J.G. Lyons, T.W. Hambley, Chem. Eur. J. 13 (2007) 2974.

[28] N. Yamamoto, A.K. Renfrew, B.J. Kim, N.S. Bryce, T.W. Hambley, J. Med. Chem. 55 (1021) (2012) 11013.

[29] A.K. Renfrew, N.S. Bryce, T.W. Hambley, Chem. Sci. 4 (2013) 3731.

[30] A.K. Renfrew, N.S. Bryce, T. Hambley, Chem. Eur. J. 21 (2015) 15224.

[31] B.J. Kim, T.W. Hambley, N.S. Bryce, Chem. Sci. 2 (2011) 2135.

[32] J.G. Tojal, J.L. Pizarro, A.G. Orad, A.R.P. Sanz, M. Ugalde, A.A. Diaz, J.L. Serra, M.I. Arriortua, T. Rojo, J. Inorg. Biochem. 86 (2001) 627.

[32] M.B. Ferrari, F. Bisceglie, G. Pelosi, P. Tarasconi, R. Albertini, A. Bonati, P. Lunghi, S. Pinelli, J. Inorg. Biochem. 83 (2001) 169.

[34] M.B. Ferrari, F. Bisceglie, G. Pelosi, P. Tarasconi, R. Albertini, P.P. Dall'Aglio, S. Pinelli, A. Pergamo, G. Sava, J. Inorg. Biochem. 98 (2004) 301.

[35] A. Ali, A.H. Mirza, A.M.S. Hossain, M. Nazimuddin, Polyhedron 20 (2001) 1045.

[36] M. Joseph, M. Kuriakose, M.R.P. Kurup, E. Suresh, A. Kishore, S.G. Bhat, Polyhedron 25 (2006) 61.

[37] M.B. Ferrari, C. Pelizzi, G. Pelosi, M.C.R. Arguelles, Polyhedron 21 (2002) 2593–2599.

[38] G. Kalaiarasi, C. Umadevi, A. Shanmugapriya, P. Kalaivani, F. Dallemer, R. Prabhakaran, Inorganica Chimica Acta 453 (2016) 547.

[39] P. Krishnamoorthy, P. Sathyadevi, R.R. Butorac, A.H. Cowley, N.S.P. Bhuvanesh, N. Dharmaraj, Dalton Trans. 41 (2012) 4423.

[40] S. Selvamurugan, R. Ramachandran, P. Vijayan, R. Manikandan, G. Prakash, P. Viswanathamurthi, K. Velmurugan, R. Nandhakumar, A. Endo, Polyhedron 107 (2016) 57

[41] K.N. Anees Rahman, J. Haribabu, C. Balachandran, N.S.P. Bhuvanesh, R. Karvembu, A. Sreekanth, Polyhedron 135 (2017) 26.

[42] S. Hosseinpour, S. A. Hosseini-Yazdi, J. White, W.S. Kassel, N.A. Piro, Polyhedron 121 (2017) 236.

[43] R.A. Bedier, T.A. Yousef, G.M. Abu El-Reash, O.A. El-Gammal, Journal of Molecular Structure 1139 (2017) 436.

[44] R. Prabhakaran, P. Kalaivani, S.V. Renukadevi, R. Huang, K. Senthilkumar, R. Karvembu, K. Natarajan, Inorg. Chem. 51 (2012) 3525.

[45] L. Ze-hua, D. Chung-Ying, L. Ji-hui, L. Young-jiang, M. Yu-hua, Y. X-Zeng, New J. Chem. 24 (2000) 1057.

[46] F. Basuli, S.M. Peng, S. Bhattacharya, Inorg. Chem. 36 (1997) 5645.

[47] C. Metcalfe, J.A. Thomas, Chem. Soc. Rev. 32 (2003) 215.

[48] M. Poyraz, M. Sari, F. Demirci, M. Kosar, S. Demirayak, O. Buyukgungor, Polyhedron 27 (2008) 2091.

[49] P.P. Netalkar, S. P. Netalkar, V. K. Revankar, Polyhedron 100 (2015) 215.

[50] L.S. Shebaldina, O.V. Kovalchukova, S.B. Strashnova, B.E. Zaitsev, T.M. Ivanova, Russ. J. Coord. Chem. 30 (2004) 38.

[51] R. Prabhakaran, K. Palaniappan, R. Huang, M. Sieger, W. Kaim, P.Viswanathamurthi, F. Dallemer, K. Natarajan, Inorg. Chim. Acta 376 (2011) 317.

[52] H.B. Shawish, M. Paydar, C.Y. Looi, Y.L. Wong, E. Movahed, S.N.A. Halim, W.F. Wong, M. Mustafa, M.J. Maah, Transition Met. Chem. 39 (2014) 81.

[53] R. Prabhakaran, P. Kalaivani, P. Poornima, F. Dallemer, G. Paramaguru, V. Vijaya Padma, R. Renganathan, R. Huange, K. Natarajan, Dalton Trans. 41 (2012) 9323.

[54] (a) N.C. Saha, R. J. Butcher, S. Chaudhuri, N. Saha, Polyhedron 22 (2003) 383 (and references there in).
(b) N.C. Saha, R. J. Butcher, S. Chaudhuri, N. Saha, Polyhedron 24 (2005) 1015.

[55] N.C. Saha, C. Biswas, A. Ghorai, U. Ghosh, S. K. Seth, T. Kar, Polyhedron 34 (2012) 1.

[56] N. C. Saha, R. Pradhan, M. Das, N. Khatun, D. Mitra, A. Samanta, A.M.Z. Slawin, A.D. Jana, J. Klanke, E. Rentschler, Journal of Coordination Chemistry 67 (2014) 286.

[57] K. Jayakumar, M. Sithambaresan, N. Aiswarya, M.R. Prathapachandra Kurup, Spectrochim. Acta A 139 (2015) 28.

[58] E. Türkkan, U. Sayin, N. Erbilen, S. Pehlivanoglu, G. Erdogan, H.U. Tasdemir, A.O. Saf, L. Guler, E.G. Akgemci, Journal of Organometallic Chemistry 831 (2017) 23.

[59] (a) N. Saha, N. Mukherjee, Polyhedron 3 (1984) 1135.
(b) M.J.S. Dewar, F.E. Kind, J. Chem. Soc. (1945) 114.
(c) Z. El-Hewehi, F. Taeger, F. Runge, J. Prakt. Chem.,18 (1962) 275.

[60] J.P. Scovil, Phosphorus, Sulfur Silicon 60 (1991) 15.

[61] A.L. Fuller, L.A.S. Scott-Hayward, Y. Li, M. Bühl, A.M.Z. Slawin, J.D. Woollins, J. Am. Chem. Soc. 132 (2010) 5799.

[62] *CrystalClear-SM Exper*t v2.1. Rigaku Americas, the Woodlands, Texas, USA, and Rigaku Corporation, Tokyo, Japan, 2015.

[63] M.C. Burla, R. Caliandro, M. Camalli, B. Carrozzini, G.L. Cascarano, L. De Caro, C. Giacovazzo, G. Polidori, R. Spagna, J. Appl. Cryst. 38 (2005) 381

[64] L. Palatinus, G. J. Chapuis, J. Appl. Cryst. 40 (2007) 786.

[65] G.M. Sheldrick, Acta Crystallogr. Sect. C. 71 (2015) 3.

[66] *CrystalStructure* v4.1. Rigaku Americas, the Woodlands, Texas, USA, and Rigaku Corporation, Tokyo, Japan, 2013.

[67] M.J. Frisch, G.W. Trucks, H.B. Schlegel, G.E. Scuseria, M.A. Robb, J.R. Cheeseman, J.A. Montgomery, T. Vreven Jr., K.N. Kudin, J.C. Burant, J.M. Millam, S.S. Iyengar, J. Tomasi, V. Barone, B. Mennucci, M. Cossi, G. Scalmani, N. Rega, G.A. Petersson, H. Nakatsuji, M. Hada, M. Ehara, K. Toyota, R. Fukuda, J. Hasegawa, M. Ishida, T. Nakajima, Y. Honda, O. Kitao, H. Nakai, M. Klene, X. Li, J.E. Knox, H.P. Hratchian, J.B. Cross, C. Adamo, J. Jaramillo, R. Gomperts, R.E. Stratmann,O. Yazyev, A.J. Austin, R. Cammi, C. Pomelli, J.W. Ochterski, P.Y. Ayala, K. Morokuma, G.A. Voth, P. Salvador, J.J. Dannenberg, V.G. Zakrzewski, S. Dapprich, A.D. Daniels, M.C. Strain, O. Farkas, D.K. Malick, A.D. Rabuck, K. Raghavachari, J.B. Foresman, J.V. Ortiz, Q. Cui, A.G. Baboul, S. Clifford, J. Cioslowski, B.B. Stefanov, G. Liu, A. Liashenko, P. Piskorz, I. Komaromi, R.L. Martin, D.J. Fox, T. Keith, M.A. Al-Laham, C.Y. Peng, A. Nanayakkara, M. Challacombe, P.M.W. Gill, B. Johnson, W. Chen, M.W. Wong, C. Gonzalez, J.A. Pople, Gaussian 09, Gaussian, Inc., Wallingford, CT, 2004.

[68] N.M. O'Boyle, A.L. Tenderholt, K.M. Langner, J. Comp. Chem. 29 (2008) 839.

[69] National Committee for Clinical Laboratory Standards (NCCLS), Approved Standard M7 A3, 3rd Edn. (1993) NCCLS, Villanova.

[70] A.W. Bauer, W.M.M. Kirby, J.C. Sherris, M. Turck, Antibiotic susceptibility testing by a standardized single disc method, Am. J. Clin. Pathol. 45 (1966) 493.

[71] W.J. Geary, Coord. Chem. Rev. 7 (1971) 81.

[72] (a) K.A. Ketchem, I. Garcia, J.K. Swearingen, A.K. El-Sawaf, E. Bermejo, A. Castiñeiras, D.X. West, Polyhedron 21 (2002) 859 (and references therein).

(b) D.X. West, J.K. Swearingen, J. Valde´s-Martı´nez, S. Herna´ndez- Ortega, A.K. El-Sawaf, F. van Meurs, A. Castiñeiras, I. Garcia, E. Bermejo, Polyhedron 18 (1999) 2919.

[73] (a) R. C. Agarwal, T. R. Rao, J. Inorg. Nucl. Chem. 40 (1978) 1177;
(b) J. R. Ferraro, Appl. Spectrosc. 23 (1969) 60.

[74] (a) A. Böttcher, T. Takeuchi, K.I. Hardcastle, T.J. Meade, H.B. Gray, Inorg. Chem., 36 (1997) 2498; b) B. Bosnich, J. Am. Chem. Soc., 90 (1968) 627.

[75] (a) O. Berradj, A. Adkhis, H. Bougherra, G. Bruno, F. Michaud, Journal of Molecular Structure , 1131 (2017) 266; b) E.B. Coropceanu, A.P. Rija, V.I. Lozan, O.A. Bologa, A.A. Boldisor, I.I. Bulhac, V.Ch. Kravtsov, P.N. Bourosh, Russ. J. Coord. Chem. 38 (2012)545; c) S.C. Nayak, P.K. Das, K.K. Sahoo, Chem. Pap. 57 (2003) 91.

[76] S. Kumar, A. Hansda, A. Chandra, A. Kumar, M. Kumar, M. Sithambaresan, Md. S.H.Faizi, V. Kumar, R.P. John, Polyhedron 134 (2017) 11 (and references therein).

[77] S. Mandal, M. Mondal, J.K. Biswas, D.B. Cordes, A.M.Z. Slawin, R.J. Butcher, M. Saha, N.C. Saha, Journal of Molecular Structure 1152 (2018) 189.

[78] N. Raman, A. Kulandaisamy, K. Jayasubramanian, Polish J. Chem. 76 (2002) 1085.

[79] B.G. Tweedy, Phytopathology 55 (1964) 910.

[80] I.C. Mendes, J.P. Moreira, A.S. Mangrich, S.P. Balena, B.L. Rodrigues. H. Beraldo, Polyhedron 26 (2007) 3263 (and references therein).

[81] N.C. Saha, S. Mandal, M. Das, N. Khatun, D. Mitra, A. Samanta, A.M.Z. Slawin, Ray J. Butcher, R. Saha, Polyhedron 68 (2014) 122.

[82] K. Helbig, C. Bleuel, G.J. Krauss, D.H. Nies, J. Bacteriol. 190 (2008) 5431.

[83] J.A. Lemire, J.J. Harrison, R.J. Turner, Nat. Rev. Microbiol. 11(2013) 371

Figure Captions:

Figure 1: (a) Structural formulation of the ligand (HMP_zNHex_2); (b) General Structural representation of Co(III) complexes; (c) General Structural representation of Ni(II) complexes.

Figure 2: Frontier molecular orbitals involved in UV–Vis absorptions in complex **I**.

Figure 3: Frontier molecular orbitals involved in UV–Vis absorptions in complex **II**.

Figure 4: View of the asymmetric unit (crystallographic numbering) of Complex **I**. Thermal ellipsoids are drawn at the 50 % probability level except for disordered carbon atoms which are drawn as spheres of arbitrary radii. Minor components of disorder omitted for clarity.

Figure 5: View of the asymmetric unit (crystallographic numbering) of Complex **II**. Thermal ellipsoids are drawn at the 50 % probability level except for disordered carbon atoms which are drawn as spheres of arbitrary radii. Minor components of disorder omitted for clarity.

Figure 6: **(a)** View down the crystallographic *a*-axis of the two-dimension hydrogen-bonded sheet formed by Complex **I**, lying in the (1 0 0) plane. Hydrogen bonds may be seen between ClO_4^- and water oxygens, and pyrazolyl nitrogens. Hydrogen atoms not involved in hydrogen bonding, minor disorder components and the C_6 chains omitted for clarity. Both positions of the disordered water molecule are included. **(b)** View down the crystallographic *b*-axis of the packing of Complex **I**, hydrogen atoms and minor disorder components omitted for clarity.

Figure 7: **(a)** View of the one-dimension hydrogen-bonded chain formed by Complex **II**, running along the *ac* diagonal axis. View is from orthogonal to the chain. Hydrogen bonds may be seen between Cl^-, water oxygens and pyrazolyl and hydrazinic nitrogens. Hydrogen atoms not involved in hydrogen bonding and minor disorder components omitted for clarity. **(b)** View down the crystallographic *b*-axis of the packing of Complex **II**, hydrogen atoms and minor disorder components omitted for clarity.

Figure 8: DFT optimised structures of the complexes **I** and **II**

Figure 9: Time dependent *in vitro* growth curves of *Enterobacter aerogenes* 10102 against the ligand and compounds: (a) MS1, (b) MS2, (c) MS3, (d) MS4, (e) MS5, (f) MS6, (g) MS7, (h) MS8, (i) MS9, (j) MS10 and (k) MS11

Figure 10: Time dependent *in vitro* growth curves of *Bacillus subtilis* 6633 against the ligand and compounds: (a) MS1, (b) MS2, (c) MS3, (d) MS4, (e) MS5, (f) MS6, (g) MS7, (h) MS8, (i) MS9, (j) MS10 and (k) MS11.

Table 1: Elemental analyses, colours and other significant physico-chemical properties of the Co(III) and Ni(II) complexes

Complex (colour)	Elemental analyses Found (calc.)				Conductivity at 30^0C $\Omega^{-1}cm^2mol^{-1}$	μ_{eff} (BM) at 300K
	%C	%H	%N	%M		
$[Co(MPzNHex_2)_2]Cl$ (red brown)	54.2 (54.4)	8.0 (8.1)	17.7 (17.6)	7.3 (7.4)	88	dia
$[Co(MPzNHex_2)_2]Br$ (red orange)	51.1 (51.5)	7.6 (7.7)	16.9 (16.7)	6.9 (7.0)	96	dia
$[Co(MPzNHex_2)_2]ClO_4 \cdot 1.5H_2O$ (red orange)	48.7 (48.8)	7.2 (7.3)	15.7 (15.8)	6.7 (6.6)	113	dia
$[Co(MPzNHex_2)_2]BF_4$ (dark red brown)	50.9 (51.1)	7.4 (7.6)	16.8 (16.5)	6.6 (6.9)	108	dia
$[Co(MPzNHex_2)_2]NO_3$ (dark red brown)	52.7 (52.6)	7.8 (7.8)	17.1 (17.0)	7.0 (7.2)	91	dia
$[Ni(HMPzNHex_2)_2]Cl_2 \cdot 2H_2O$ (green)	49.3 (49.8)	7.4 (7.6)	16.4 (16.1)	6.9 (6.8)	202	2.88
$[Ni(HMPzNHex_2)_2]Br_2$ (light green)	46.8 (46.9)	7.0 (7.2)	15.3 (15.2)	6.5 (6.4)	182	3.20
$[Ni(HMPzNHex_2)_2](ClO_4)_2$ (dark green)	45.0 (45.0)	6.8 (6.9)	14.6 (14.6)	6.0 (6.1)	195	3.08
$[Ni(HMPzNHex_2)_2] (BF_4)_2$ (dark green)	46.3 (46.2)	7.2 (7.1)	15.0 (15.0)	6.2 (6.3)	172	2.95
$[Ni(HMPzNHex_2)_2](NO_3)_2$ (light green)	48.8 (48.8)	7.6 (7.5)	15.9 (15.8)	6.5 (6.6)	177	3.18

Table 2: Vertical excitations with band position, oscillator strength and character assignments

Complex	Experimental wave length (nm)	Wave length obtained from TD-DFT (nm)	Oscillator strength (f)	Maximum orbital contribution	percentage (%)	Transition Assignment
I	391.49	359.67	0.0311	HOMO- > L+2	36%	L → M+L
	325.51	292.93	0.13	H-1- > LUMO	50%	L → L
	227.82	234.97	0.13	H- 4- > LUMO	60%	L → L
II	359.15	322.86	0.044	HOMO- > LUMO	70%	L → M (Ligand assisted)
	307.39	288.59	0.28	H-1- > L+1	38%	L → L
	223.29	209.4	0.15	H-1- > L+4	57%	L → L

Table 3: ^{1}H NMR data (in $CDCl_3$) for HMP_zNHex_2 and its Co(III) complexes relative to TMS

Compound	-N*H* (imino)	Azomethine -C-*H*	Ring (P_z) N^1-*H*	Ring (P_z) C_5-C*H*$_3$	Ring (P_z) C_4-*H*	-N-(C*H*$_2$-C_5)$_2$	-N-(C-C*H*$_2$-C_4)$_2$	-N-(C_2-(C*H*$_2$)$_3$-C)$_2$	-N-(C_5-*CH*$_3$)$_2$
HMP_zNHex_2	11.51	7.27	12.83	2.34	6.12	3.64	1.65	3 (1.23)	0.79
$[Co(MP_zNHex_2)_2]Cl$		8.39	12.99	2.58	6.16	3.78	1.70	3 (1.27)	0.81
$[Co(MP_zNHex_2)_2]Br$		8.42	12.89	2.49	6.19	3.76	1.66	3 (1.27)	0.84
$[Co(MP_zNHex_2)_2]ClO_4 \cdot 1.5H_2O$		8.39	12.99	2.59	6.17	3.74	1.67	3 (1.27)	0.89
$[Co(MP_zNHex_2)_2]BF_4$		8.41	12.92	2.52	6.15	3.71	1.69	3 (1.27)	0.88
$[Co(MP_zNHex_2)_2]NO_3$		8.44	12.95	2.57	6.18	3.73	1.71	3 (1.27)	0.83

Table 4: Crystal data and structure refinement parameters for **Complex I** & **Complex II**

	$[Co(MP_zNHex_2)_2]ClO_4 \cdot 1.5H_2O$ **(I)**	$[Ni(HMP_zNHex_2)_2]Cl_2 \cdot 2H_2O$ **(II)**
Empirical formula	$C_{36}H_{67}ClCoN_{10}O_{5.5}S_2$	$C_{36}H_{70}Cl_2N_{10}NiO_2S_2$
Formula weight	886.50	868.74
Crystal description	orange prism	green prism
Crystal size [mm^3]	0.18×0.12×0.05	0.27×0.10×0.03
Temperature [K]	125	125
Wavelength [Å]	0.71075	0.71075
Crystal system	monoclinic	triclinic
Space group	*C*2/*c*	*P*-1
a [Å]	41.887(6)	10.867(4)
b [Å]	9.0663(11)	13.428(5)
c [Å]	25.397(3)	17.055(5)
α [°]		77.16(2)
β [°]	105.335(3)	74.464(19)
γ [°]		86.80(2)
Volume [$Å^3$]	9301(2)	2337.8(14)
Z	8	2
ρ (calc) [g/cm^3]	1.266	1.234
μ [mm^{-1}]	0.556	0.659
F(000)	3784	932
Reflections collected	60145	30168
Independent reflections (R_{int})	8502 (0.0779)	8492 (0.2002)
Data/restraints/parameters	8502 / 168 / 563	8492 / 423 / 498
GOF on F^2	1.022	1.069
R_1 [$I > 2\sigma(I)$]	0.0571	0.1707
wR_2 (all data)	0.1645	0.4666
Largest diff. peak/hole [$e/Å^3$]	0.79, -0.61	2.53, -1.04

Table 5. Selected bond lengths (Å) and bond angles (°) of $C_{36}H_{67}ClCoN_{10}O_{5.5}S_2$ **(I)** and $C_{36}H_{70}Cl_2N_{10}NiO_2S_2$**(II)** .

Bond lengths	Complex_**I**		Complex_**II**	
	Crystal	Calculated	Crystal	Calculated
M1-S10	2.2057(11)	2.2822	2.417(5)	2.28268
M1-S40	2.2182(11)	2.28026	2.413(5)	2.80159
M1-N1	1.936(3)	1.97245	2.071(14)	1.96424
M1-N31	1.935(3)	1.97269	2.046(15)	2.59343
M1-N8	1.899(3)	1.93754	2.042(12)	1.93087
M1-N38	1.902(3)	1.9393	2.046(12)	1.96702
N9-C10	1.331(5)	1.32957	1.36(2)	1.36435
N39-C40	1.321(5)	1.33045	1.36(2)	1.37235
S10-C10	1.741(4)	1.766448	1.681(15)	1.72823
S40-C40	1.747(4)	1.76612	1.716(16)	1.69979
Angle				
S10-M1-N31	89.98(10)	90.604	91.3(4)	99.769
S40-M1-N1	91.32(9)	90.873	92.4(4)	88.017
S10-M1-N8	85.59(9)	84.792	80.2(4)	85.555
S40-M1-N38	85.40(10)	84.892	80.3(4)	75.953
S10-M1-N1	167.28(9)	166.282	157.7(4)	166.192
S40-M1-N31	167.08(10)	166.44	157.5(4)	145.881
S10-M1-N38	96.85(9)	95.89	104.7(4)	94.521
S40-M1-N8	97.14(9)	95.607	102.7(4)	109.352
N1-M1-N8	81.80(12)	81.702	77.7(5)	81.007
N8-M1-N31	95.75(13)	97.764	99.6(5)	174.622
N1-M1-N38	95.68(13)	97.592	97.2(5)	98.560
N31-M1-N38	81.69(14)	81.711	77.2(6)	74.681
N1-M1-N31	89.65(13)	88.858	89.5(6)	79.588
N8-M1-N38	176.45(13)	179.136	174.1(6)	174.622
N8-N9-C10	111.2(3)	113.388	117.0(12)	118.506
N38-N39-C40	112.1(3)	113.311	119.3(13)	123.006
S10-M1-S40	91.87(4)	92.826	95.32(19)	99.484

(M1= Co1= Ni1)

Table 6: Hydrogen bonding distances (Å) and angles (°)

D-H...A	D.....A	D-H	H.....A	∠D-H...A
Complex I				
N2-H2⋯O1A	3.037(10)	0.935(19)	2.19(3)	151(4)
N2-H2⋯O62	2.792(7)	0.935(19)	1.93(3)	152(4)
N32-H32⋯O61	2.810(5)	0.972(19)	1.85(2)	171(4)
O61⋯ O1[1]	2.783(9)			
O61⋯ O4[2]	2.830(10)			
O62⋯O2[3]	3.063(11)			
O62⋯O2	3.010(13)			
Complex II				
N2-H2⋯O61	2.713(19)	0.98	1.73	177.8
N9-H9⋯Cl2	3.179(13)	0.98	2.42	133.6
N32-H32⋯O62	2.748(17)	0.98	1.77	175.5
N39-H39⋯Cl1[4]	3.198(16)	0.98	2.41	136.9
O61⋯Cl1[5]	3.127(14)			
O61⋯Cl1[4]	3.132(15)			
O62⋯Cl2[6]	3.114(12)			
O62⋯Cl2	3.127(14)			

Symmetry Operators: (1) 1–X, 1+Y, ½–Z; (2) X, 1+Y, Z; (3) 1–X, –Y, 1–Z
(4) –1+X, Y, Z; (5) 1–X, 1–Y, –Z; (6) 1–X, 1–Y, 1–Z

Table 7: The minimum inhibitory concentrations (MIC, µg/mL) of the ligand and the synthesized Co(III) & Ni(II) compounds against three Gram negative bacteria (*Salmonella enterica ser. typhi* SRC, *Proteus vulgaris* OX19, *Enterobacter aerogenes* 10102) and one Gram positive bacteria (*Bacillus subtilis* 6633)

Organisms	**MS1$^{\alpha}$**	**MS2$^{\beta}$**	**MS3$^{\beta}$**	**MS4$^{\beta}$**	**MS5$^{\beta}$**	**MS6$^{\beta}$**	**MS7$^{\gamma}$**	**MS8$^{\gamma}$**	**MS9$^{\gamma}$**	**MS10$^{\gamma}$**	**MS11$^{\gamma}$**	**AM***
P. vulgaris OX19	200	875	725	650	375	450	1350	1575	775	1000	1375	125
B. subtilis 6633	300	600	575	350	225	575	1200	1375	1075	900	1450	30
S. typhi SRC	475	1375	1225	650	575	700	1300	1450	650	625	1500	35
E. aerogenes 10102	500	1675	1400	675	600	1050	1650	1525	950	975	1025	280

AM*= Amoxicillin – the antibiotic which was used as the standard antimicrobial agent in the present study.$^{\alpha}$MS1= HMP_zNHex_2. $^{\beta}[Co(MP_zNHex_2)_2]X$ (X= Cl, Br, ClO_4, BF_4 and NO_3 for MS2, MS3, MS4, MS5 and MS6, respectively. $^{\gamma}[Ni(HMP_zNHex_2)_2]Y_2$ (Y= Cl, Br, ClO_4, BF_4 and NO_3 for MS7, MS8, MS9, MS10 and MS11, respectively.

Table 8: Growth inhibition zone diameter (mm) developed when different bacterial strains were subjected to respective MICs of the ligand and Co(III) & Ni(II) compounds tested. The means of inhibition zone measured were presented with respected standard deviation.

Organisms	**MS1**	**MS2**	**MS3**	**MS4**	**MS5**	**MS6**	**MS7**	**MS8**	**MS9**	**MS10**	**MS11**	**AM***
P. vulgaris OX19	2.3±0.1	2.7±0.3	2.3±0.1	2.6±0.2	2.5±0.2	2.1±0.1	3.3±0.2	3.0±0.1	3.7±0.3	3.1±0.4	2.3±0.2	7.9±0.3
B. subtilis 6633	2.7±0.2	4.3±0.3	3.6±0.4	3.3±0.1	2.6±0.2	4.4±0.4	2.7±0.3	2.3±0.1	2.6±0.2	3.4±0.4	3.3±0.1	8.4±0.4
S. typhi SRC	2.5±0.1	3.1±0.2	3.9±0.3	6.8±0.2	2.1±0.3	1.9±0.1	6.9±0.1	6.2±0.2	5.9±0.4	6.8±0.2	9.1±0.3	9.1±0.2
E. aerogenes 10102	5.3±0.3	4.3±0.5	3.3±0.2	4.3±0.4	3.7±0.2	2.7±0.1	3.7±0.3	5.4±0.2	7.3±0.4	5.3±0.1	5.7±0.2	8.5±0.3

AM*= Amoxicillin, the antibiotic which was used as the standard antimicrobial agent in the present study.

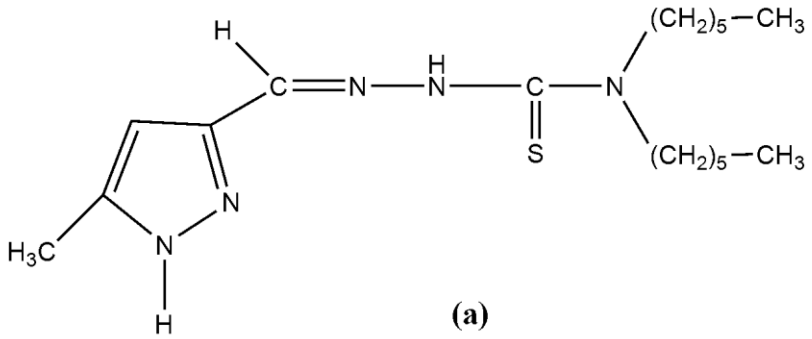

(a)

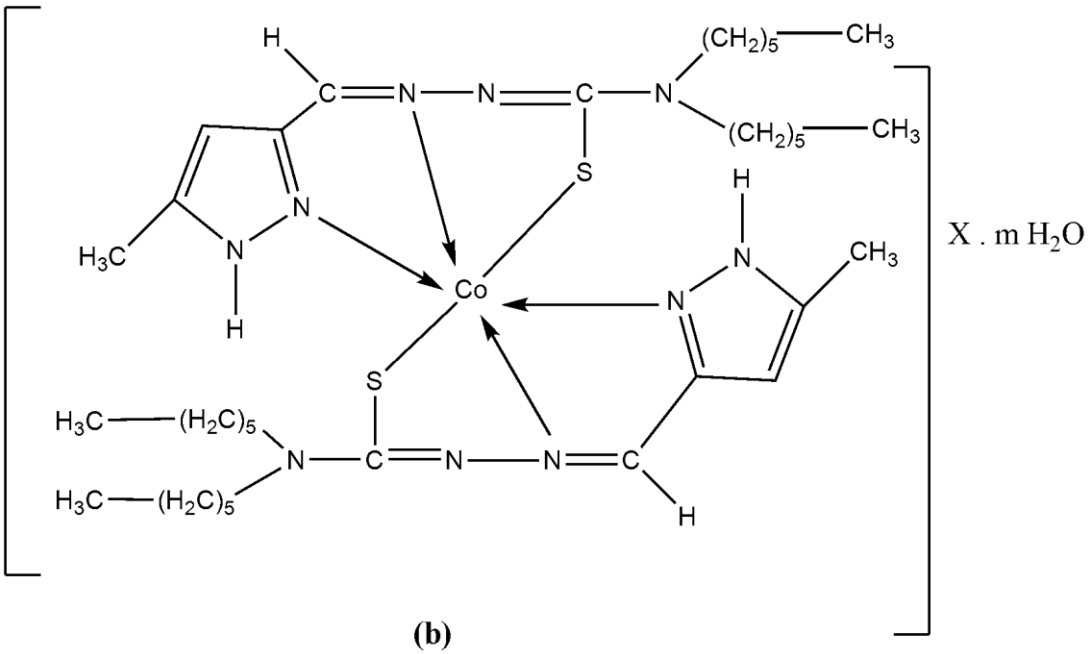

(b)

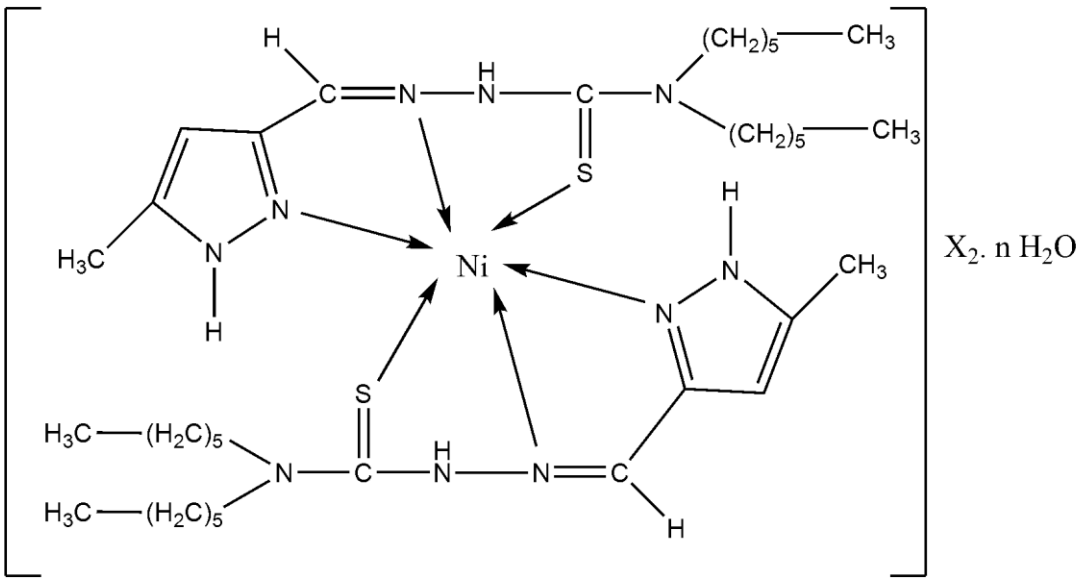

(c)

Figure 1

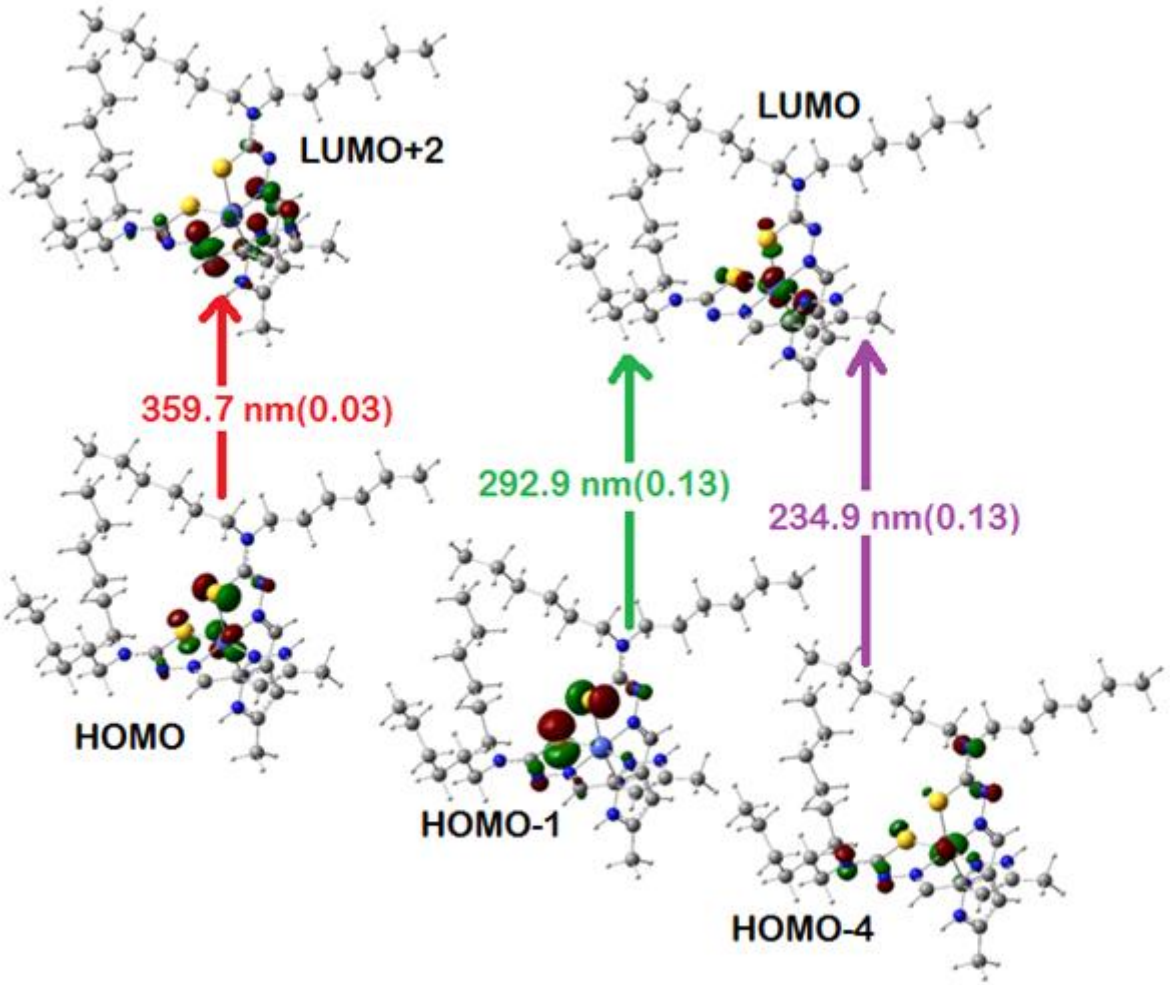

Figure 2

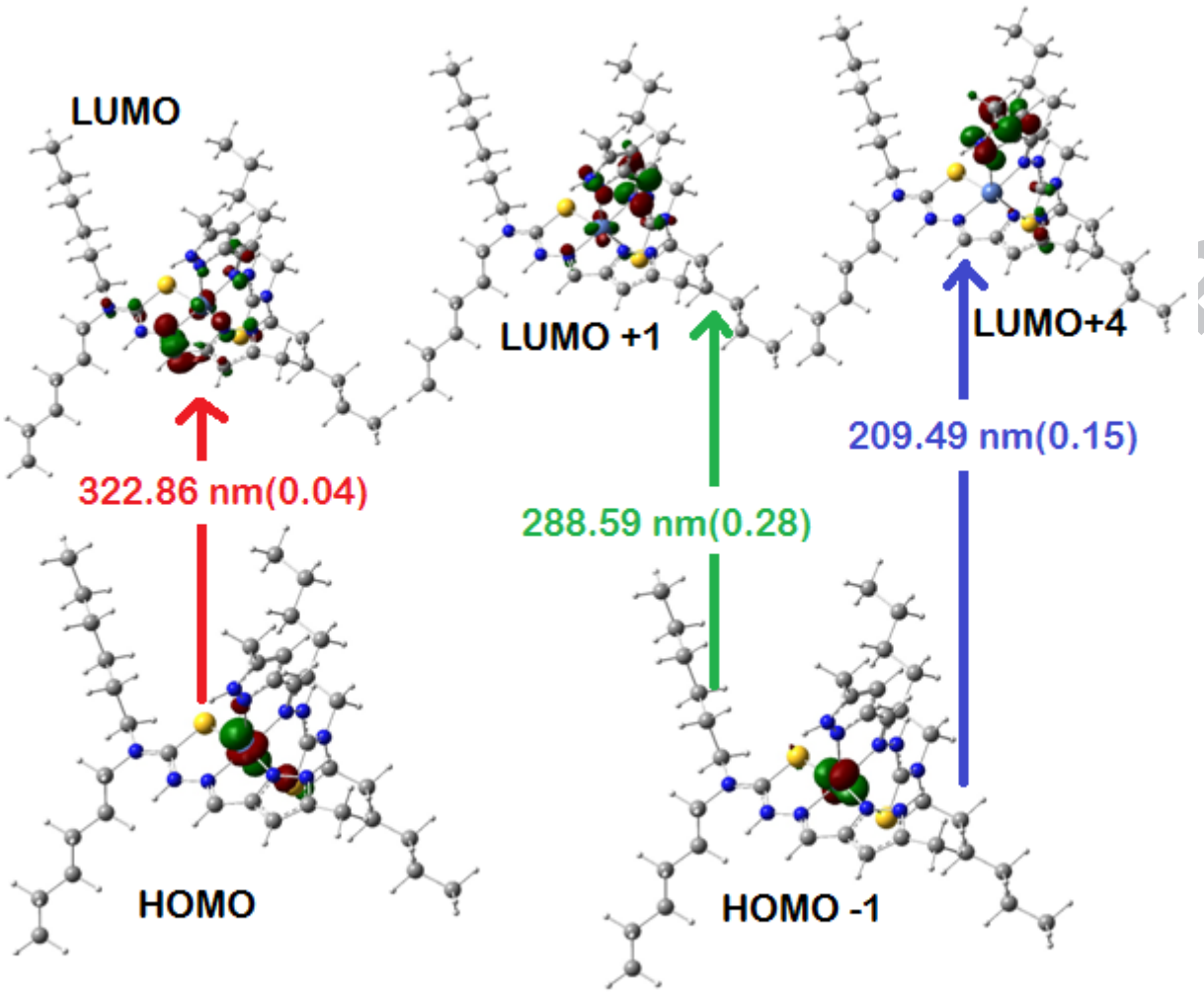

Figure 3

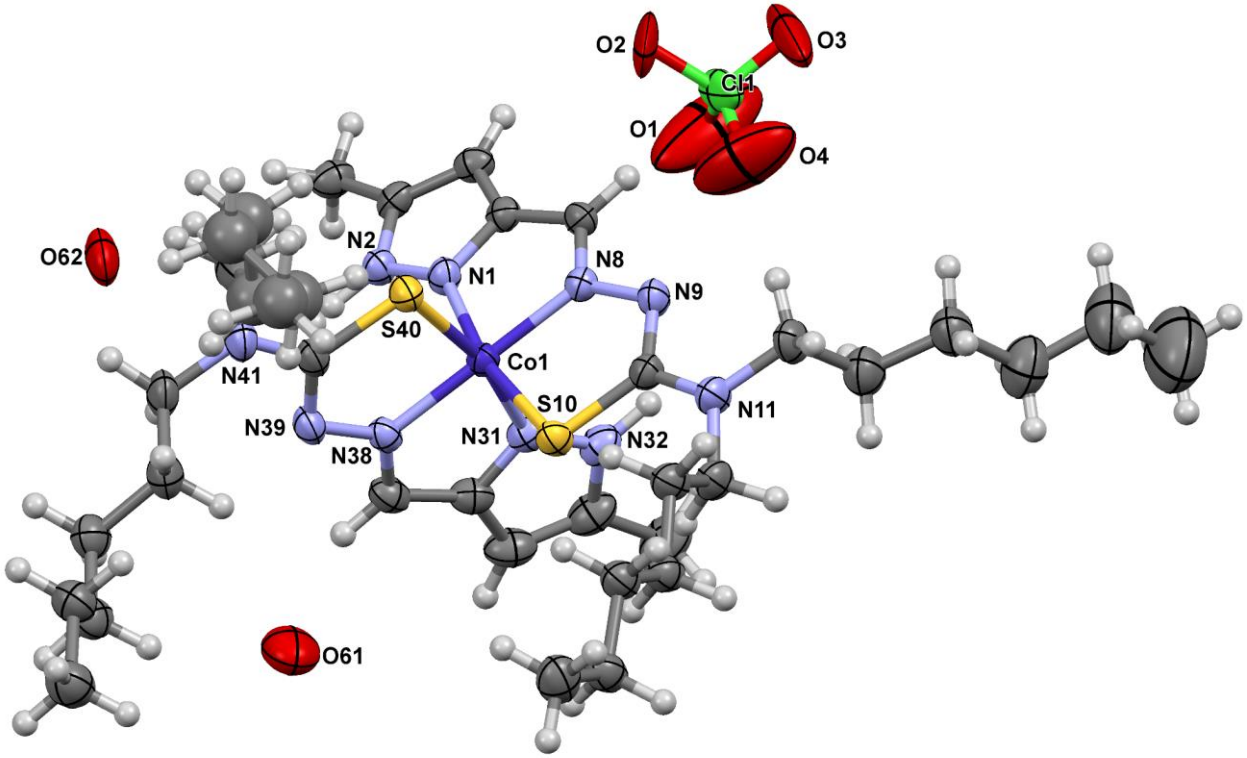

Figure 4

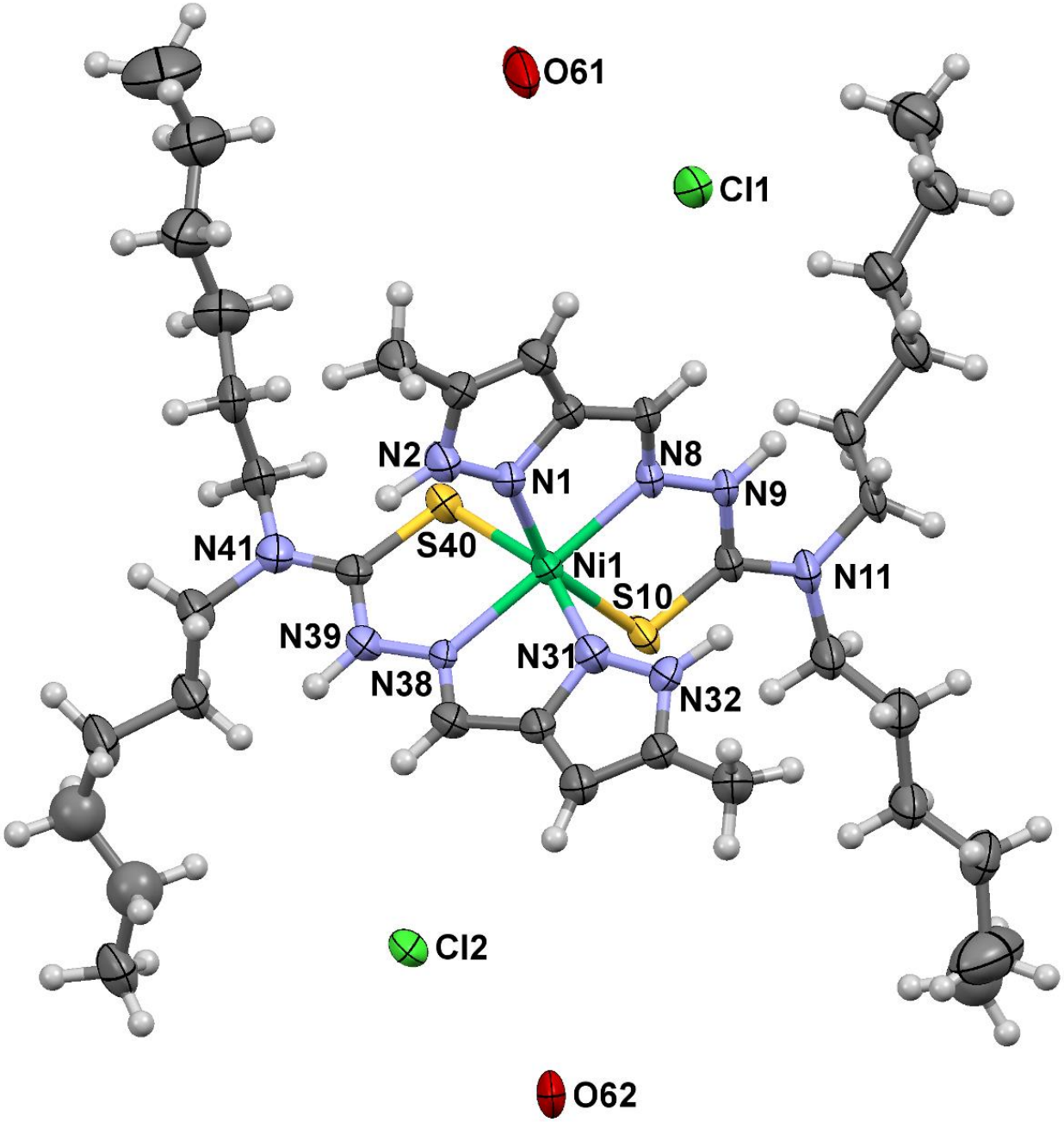

Figure 5

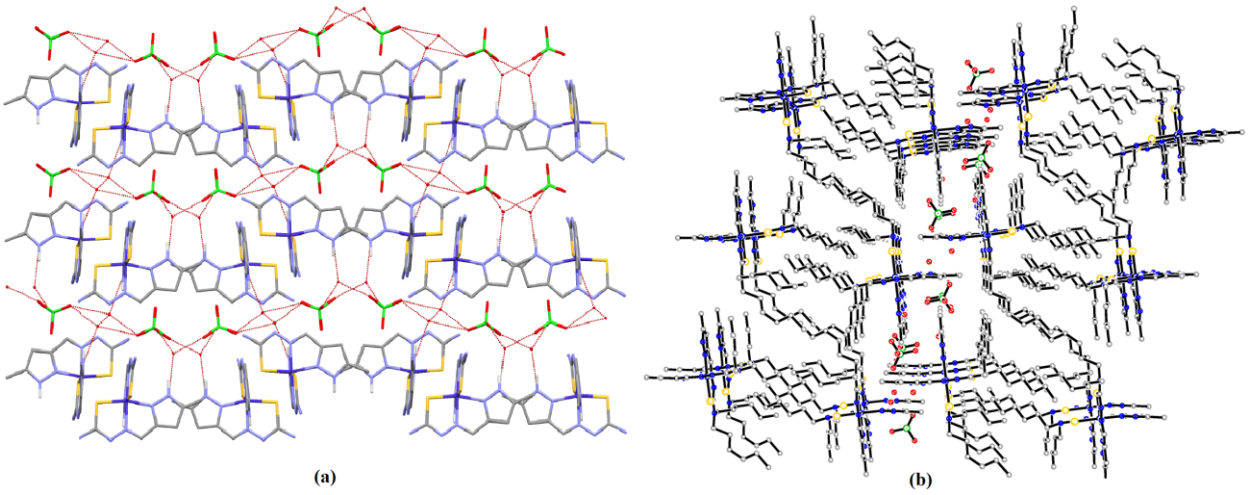

(a) (b)

Figure 6

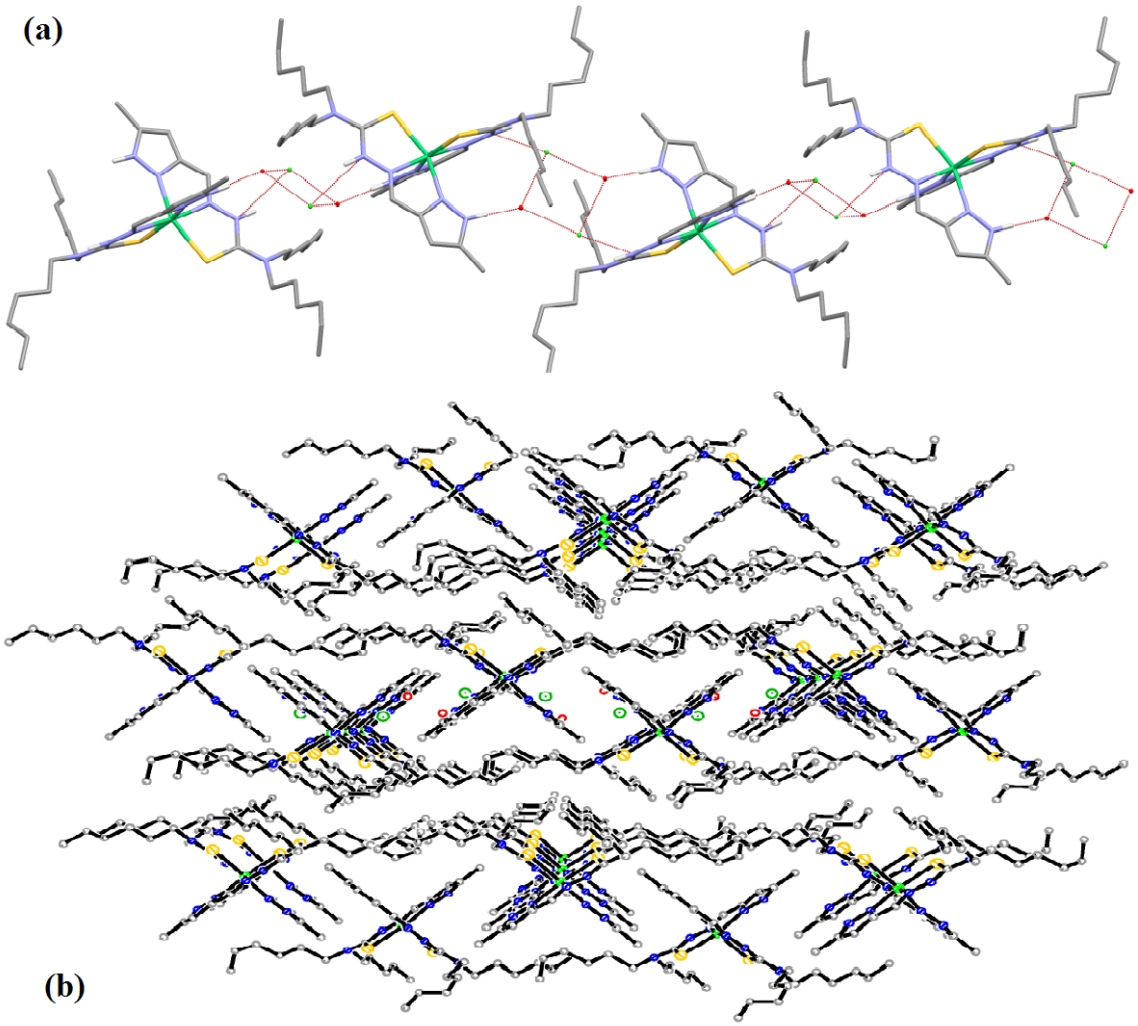

Figure 7

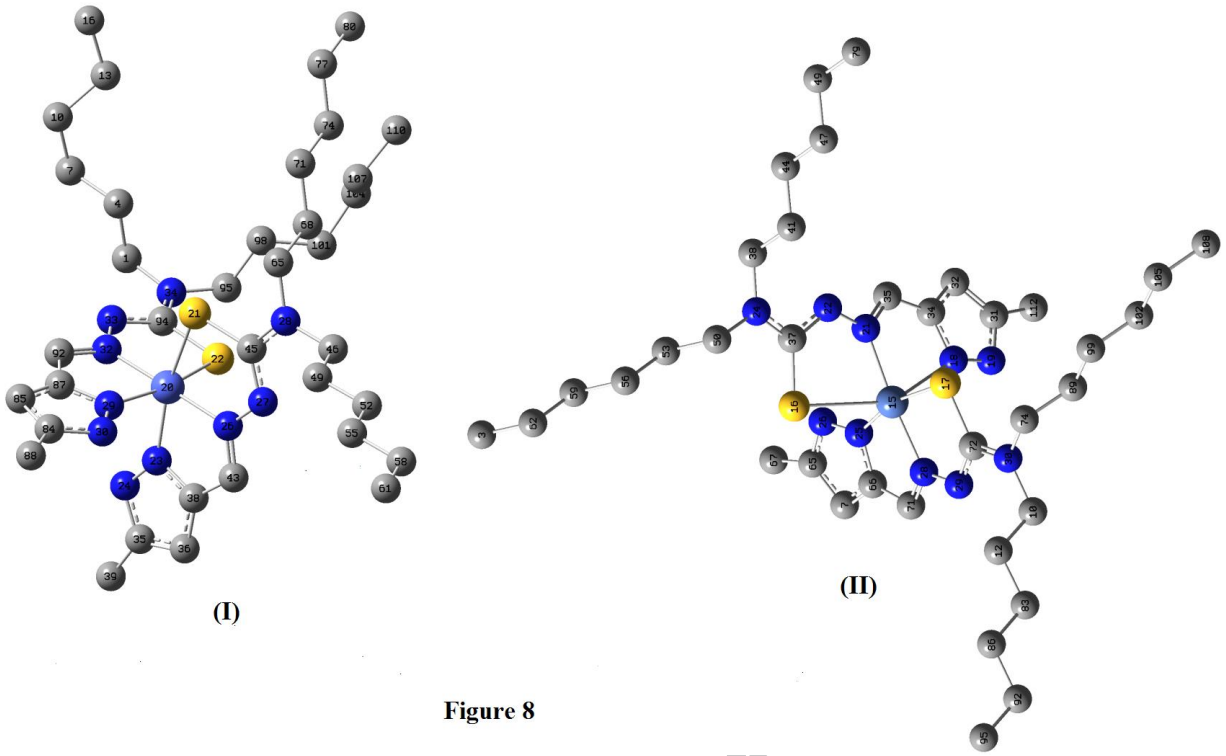

(I) (II)

Figure 8

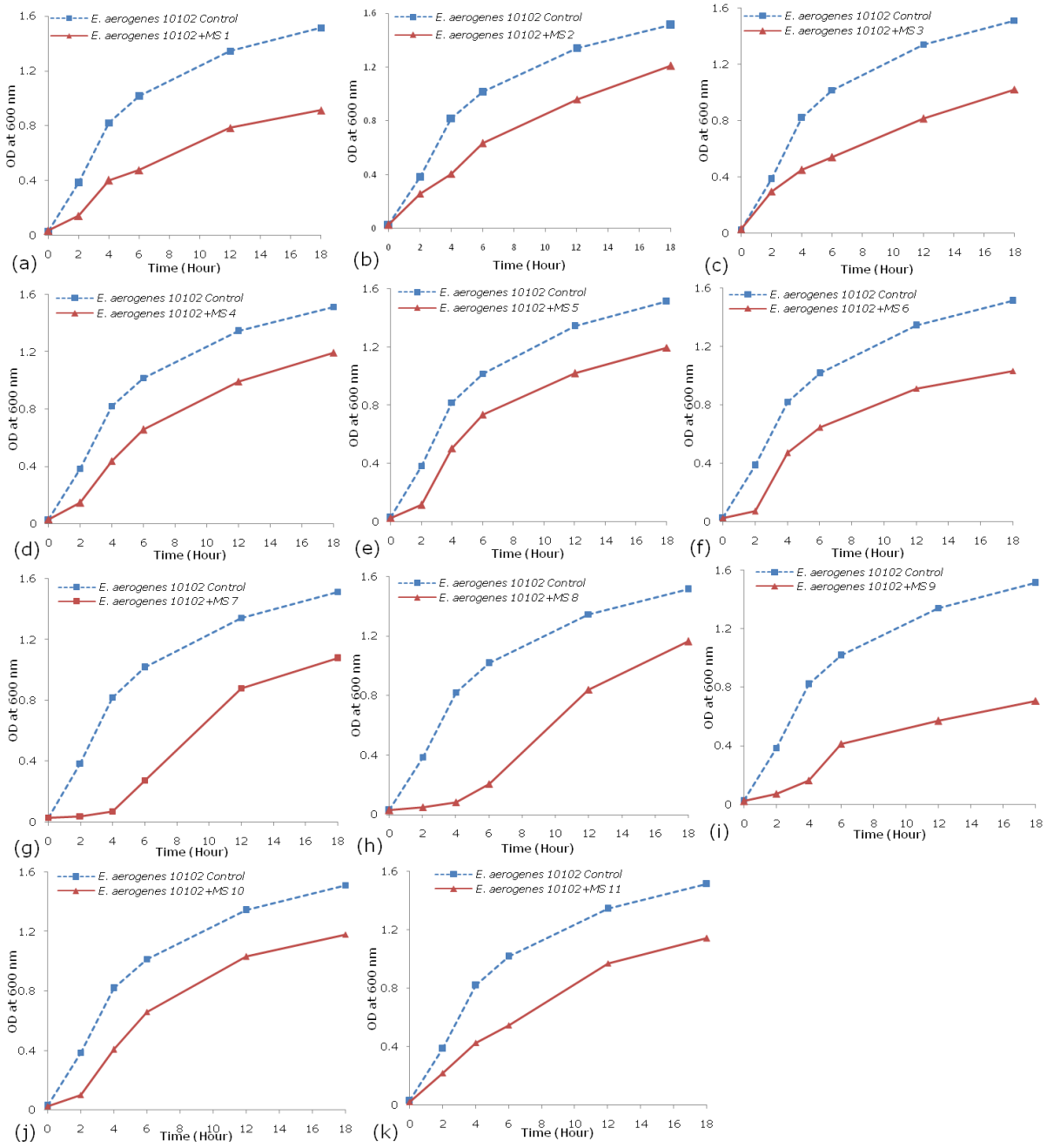
E. aerogenes 10102 Control
E. aerogenes 10102+MS 1
E. aerogenes 10102+MS 2
E. aerogenes 10102+MS 3
E. aerogenes 10102+MS 4
E. aerogenes 10102+MS 5
E. aerogenes 10102+MS 6
E. aerogenes 10102+MS 7
E. aerogenes 10102+MS 8
E. aerogenes 10102+MS 9
E. aerogenes 10102+MS 10
E. aerogenes 10102+MS 11
OD at 600 nm
Time (Hour)
(a)
(b)
(c)
(d)
(e)
(f)
(g)
(h)
(i)
(j)
(k)

Figure 9

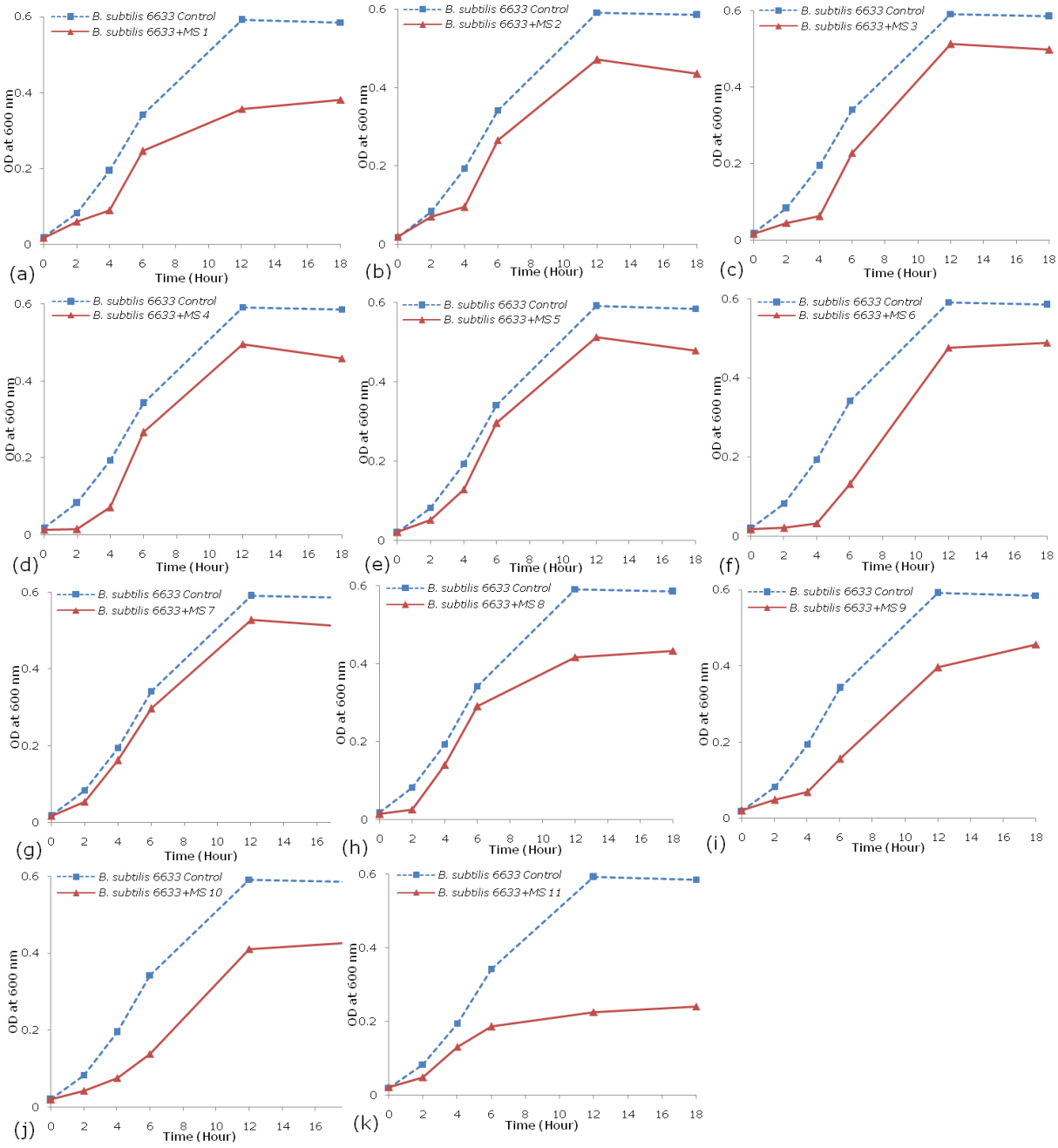
B. subtilis 6633 Control
B. subtilis 6633+MS 1
B. subtilis 6633+MS 2
B. subtilis 6633+MS 3
B. subtilis 6633+MS 4
B. subtilis 6633+MS 5
B. subtilis 6633+MS 6
B. subtilis 6633+MS 7
B. subtilis 6633+MS 8
B. subtilis 6633+MS 9
B. subtilis 6633+MS 10
B. subtilis 6633+MS 11
OD at 600 nm
Time (Hour)
(a)
(b)
(c)
(d)
(e)
(f)
(g)
(h)
(i)
(j)
(k)

Figure 10

A new pyrazole containing Thiosemicarbazone ligand and its octahedral Co(III) and Ni(II) complexes have been synthesized & characterized. The reported NNS tridentate ligand (HMP_zNHex_2) binds with the metal ion via the pyrazolyl tertiary nitrogen, the azomehine nitrogen and the sulphur in its thione / thiol form. The structural conformations of Co(III) and Ni(II) complexes have been established by X-ray studies and DFT calculations of $[Co(MP_zNHex_2)_2]ClO_4 \cdot 1.5H_2O$ (**I**) and $[Ni(HMP_zNHex_2)_2]Cl_2 \cdot 2H_2O$ (**II**). The detailed antimicrobial activities of the title ligand and all the complexes have been reported.

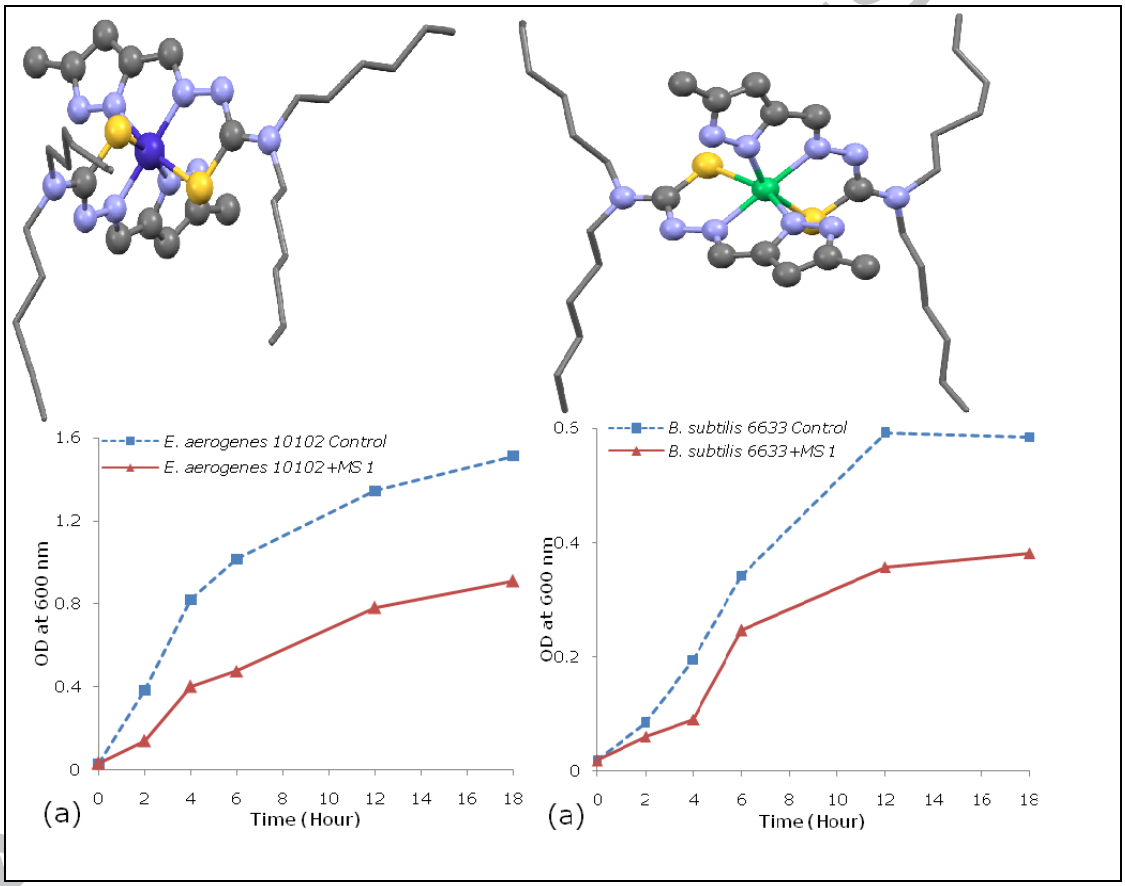

Highlights (for review)

Syntheses, physico-chemical and spectroscopic characterizations of new pyrazole containing Thiosemicarbazone ligand and its Co(III) and Ni(II) complexes have been reported.

X-ray crystallographic studies on Complex **I** and **II** have authenticated the structures of the complexes as envisaged from spectroscopy.

Antimicrobial activities of the complexes against some Gram positive and Gram negative bacteria have been reported, and the complexes have been found to be the potential antimicrobial agents in broad spectrum against the both.